INL/EXT-16-40122

Characterizing the Benefits of Seismic Isolation for Nuclear Structures: A Framework for Risk-Based Decision Making

INL Seismic Research Group

November 2016

The INL is a U.S. Department of Energy National Laboratory
operated by Battelle Energy Alliance

INL/EXT-16-40122

Characterizing the Benefits of Seismic Isolation for Nuclear Structures: A Framework for Risk-Based Decision Making

Chandrakanth Bolisetti, INL
Chingching Yu, MCEER/UB
Justin Coleman, INL
Ben Kosbab, SC Solutions
Andrew Whittaker, MCEER/UB

November 2016

Idaho National Laboratory
Idaho Falls, Idaho 83415

www.inl.gov

Prepared for the
U.S. Department of Energy
Under DOE Idaho Operations Office
Contract DE-AC07-05ID14517

EXECUTIVE SUMMARY

Seismic isolation has been implemented in many civil structures, including buildings, bridges, liquid natural gas tanks, and off shore oil platforms, both in the United States and other countries, to mitigate the damaging effects of earthquakes. Seismic isolation has also been implemented in nuclear structures in France and South Africa, but not yet in the United States, in either Department of Energy facilities or commercial nuclear power plants (NPPs). This is primarily due to a lack of guidelines, and codes and standards for the analysis, design and construction specific to seismically isolated nuclear structures. However, seismic isolation of nuclear structures has seen increased research interest in the recent years and the forthcoming version of the national consensus standard America Society of Civil Engineers (ASCE) Standard 4-16 (ASCE, 2016) "Seismic analysis of safety related nuclear structures", recently incorporated language and commentary (Chapter 12) for seismically isolating surface or near-surface-mounted nuclear facilities, including NPPs.

Seismic isolation substantially reduces horizontal seismic loads (demands) on structures, systems, and components. Reduction in demand results in four potential benefits: (1) *economic*: reduction in capital cost, (2) *increased safety*: reduction in the mean annual frequency of unacceptable performance, (3) *insurance*: protection against increases in the known seismic hazard after construction by minimizing the effort to re-qualify and re-certify structures, systems and components, and (4) *recertification*: the opportunity to certify an existing NPP design for a region of higher seismic hazard.

Item (2) above, an increase in safety (reduction of seismic risk), was explored in Huang et al. (2008b) where it was demonstrated that the implementation of seismic isolation reduced seismic risk in nuclear power plant structures. However, studies that assess item (1) have not been performed although the use of isolation may lead to large reductions in the capital cost of safety-related nuclear facilities. Funding provided by Nuclear Safety Research and Development in the Department of Energy (DOE) has allowed the authors of this report to develop a framework for assessing the economic benefits and reductions in seismic risk afforded by the use of seismic (base) isolation. The framework includes probabilistic risk assessment and estimation of overnight capital costs of a sample generic DOE nuclear facility (GDNF).

Risk assessments are performed and cost estimates are made for the GDNF for three cases:

1. A GDNF located at a site of low to moderate seismic hazard and constructed on a conventional (non-isolated) foundation
2. A GDNF located at a site of high seismic hazard and constructed on a conventional foundation
3. A GDNF located at the same site of high seismic hazard as Case 2, but seismically isolated

In this study, the DOE site at Idaho National Laboratory (INL) is chosen for the site of low to moderate seismic hazard (Case 1). The Los Alamos National Laboratory (LANL) is chosen as the site of high seismic hazard (Cases 2 and 3).

The seismic risk calculations presented in this report for INL and LANL sites demonstrate the benefits of isolation. For the components assumed to populate the GDNF and the hypothetical event trees and fault trees, the introduction of horizontal isolation reduces the risk (mean annual frequency of unacceptable performance) by many orders of magnitude: to 10^{-11} and 10^{-12} here. Such a dramatic reduction in risk may not be needed because risk numbers on par (or lower) than those targeted for DOE facilities and commercial nuclear power plants could be achieved by a combination of a) seismic isolation, and b) installed structures, systems and components (SSCs) with substantially less ruggedness than those required to meet risk targets in conventionally founded (non-isolated) structures. Construction

cost will increase when isolators and an additional basemat/moat wall/pedestals are added, but these will generally be a very small fraction of the total construction cost. Substantial savings in the cost of installed SSCs will result from the implementation of isolation and the corresponding large reductions in seismic demand, especially in the horizontal direction.

For the GDNF considered here, the total construction cost increases with design peak ground acceleration (PGA). (Design PGA is not the best estimator of seismic demand, but it is used here because the prior studies by Stevenson (1981, 2003) that form the basis of the cost calculations presented in this report use PGA as the seismic design metric.) Figure E-1 shows that the cost of the isolated GDNF is greater than that of the conventional structure when the design PGA is small, which is an expected result because the seismic design penalty for the SSCs is very small, and there is additional construction cost to implement isolation, as noted above. However, beyond a threshold value of PGA, which is about 0.2 g for this structure, isolation becomes cost effective. The threshold value would decrease with an increase in the fraction of the total cost of the supported SSCs.

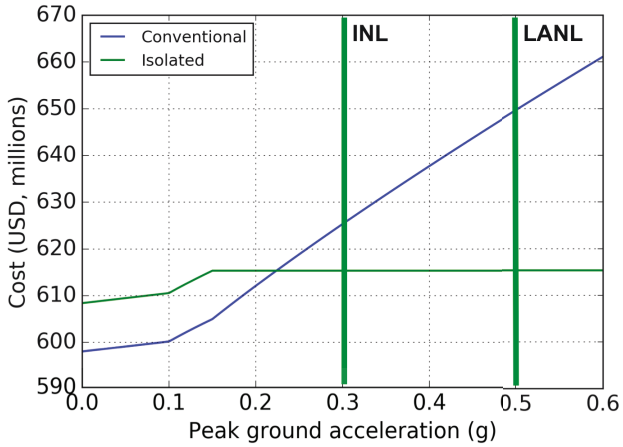

Figure E-1: Total cost as function of the design PGA of conventional and isolated variants of the GDNF

CONTENTS

FIGURES

TABLES

1. INTRODUCTION

1.1 Seismic isolation

Base isolation has been implemented in many civil structures, including buildings, bridges, liquid natural gas tanks, and off shore oil platforms, both in the United States and other countries, to mitigate the damaging effects of earthquakes. Seismic isolation has also been implemented in nuclear structures in France and South Africa, but not yet in the United States, in either Department of Energy (DOE) facilities or Nuclear Regulatory Commission- (NRC-) regulated nuclear power plants (NPPs) due to a lack of guidelines, and codes and standards for the analysis, design and construction specific to seismically isolated nuclear structures. The potential benefits of seismically isolating nuclear structures include 1) economic: reduction in capital cost, 2) increased safety: reduction in the mean annual frequency of unacceptable performance, 3) insurance against changes in the known seismic hazard: mitigate or eliminate the need to redesign or re-certify if the seismic hazard increased due to new knowledge, and 4) the opportunity to certify an existing NPP design for a region of higher seismic hazard.

Seismic isolation of nuclear structures has seen increased research interest in the recent years, particularly since the implementation of the certified design regulatory approaches in 10 CFR 52, "Licenses, certifications, and approvals for nuclear power plants." The US Nuclear Regulatory Commission (USNRC) is currently in the process of publishing a NUREG/CR report (Kammerer et al., forthcoming) that investigates and discusses the implementation of seismic isolation in large light water reactor structures. A recent INL study (Kammerer et al. 2015) also documented the regulatory gaps and research challenges that need to be addressed for licensing seismically isolated advanced reactors. The forthcoming version of the national consensus standard America Society of Civil Engineers (ASCE) Standard 4-16 (ASCE 2016) "Seismic analysis of safety related nuclear structures", recently incorporated language and commentary (Chapter 12) for seismically isolating a surface or near-surface-mounted nuclear facilities, including NPPs: see Figure 1-1.

The primary benefit of seismic isolation is the substantial reduction in the horizontal demands on SSCs during earthquake shaking that translates into reductions in seismic risk. Related benefits include potential cost saving costs for the construction of the facility and its equipment. Huang et al. (2008b) demonstrated a 70% reduction in seismic demands in secondary systems and a seismic risk reduction of about three orders of magnitude in a nuclear power plant structure due to the addition of an isolation system. In the nuclear power plant industry, seismic isolation could permit reactor designs certified for regions of low to moderate seismic hazard to be constructed in regions of high seismic hazard with minimal design modifications. Much of the re-licensing process and the additional seismic qualification for a site of higher seismic hazard would be avoided, which in turn would lead to significant reductions in cost and time.

Possible reductions in construction cost associated with the implementation of seismic isolation have not yet been characterized in a way that could assist decision makers to assess the costs and benefits of implementing seismic isolation. Although the reduction in seismic risk has been demonstrated (e.g., Huang et al. 2008b), no studies have been performed to estimate the reduction in cost, if any. The study presented in this report addresses this gap and provides a calculation framework for others to follow, on a project-specific basis, to characterize the costs and benefits of seismic isolation. The development of the calculation framework was made possible by funding from the Department of Energy's program for Nuclear Safety Research and Development.

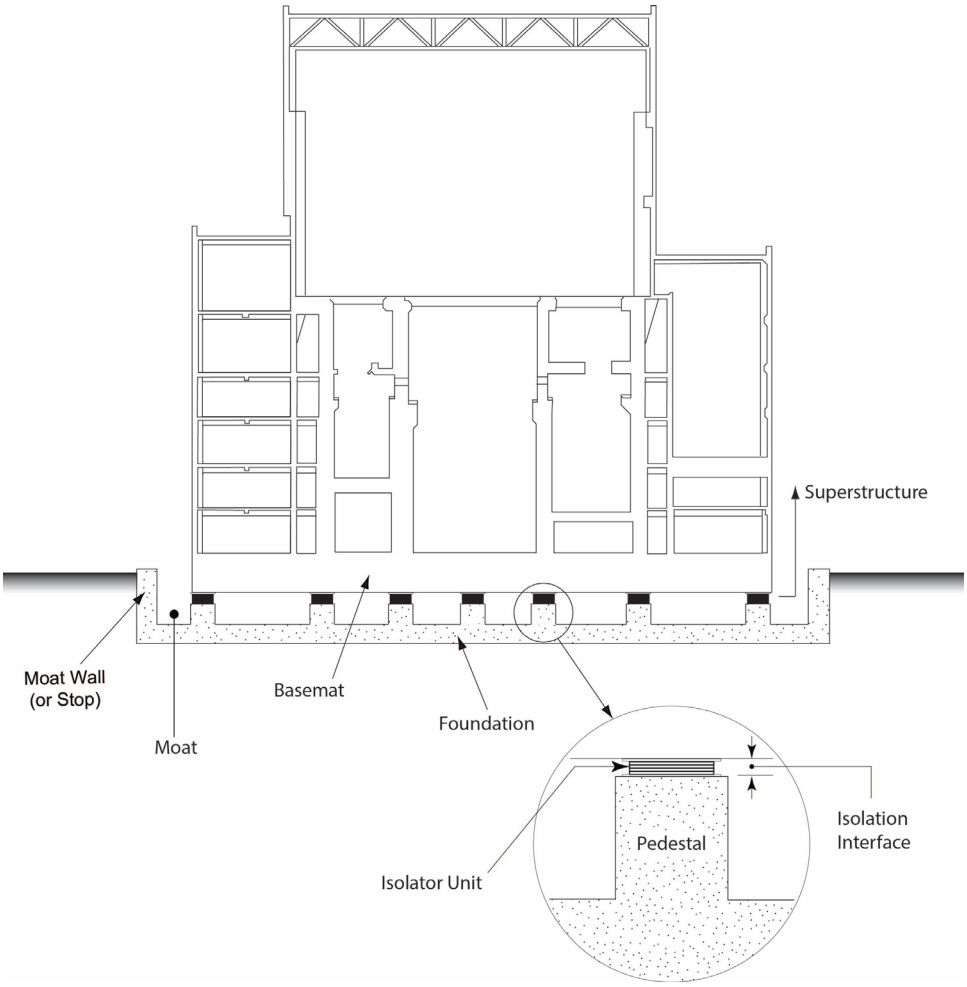

Figure 1-1: Seismic isolation of a light water reactor (Kammerer et al. 2015)

1.2 Objectives of the study

This report provides a calculation framework to characterize the benefits of isolation in terms of construction cost and risk reduction. This framework is applied to a generic nuclear facility at the Idaho National Laboratory, termed hereafter as a Generic Department of Energy Nuclear Facility (GDNF). It could be applied to any other safety-related nuclear structure including a nuclear power plant. The GDNF consists of a two-story concrete building on a near-surface conventionally founded (i.e., not seismically isolated) basemat.

The study presented in this report assesses the benefits of seismically isolating the GDNF by comparing the total costs and the risk of loss of confinement due to an earthquake in three cases:

1. Case 1: GDNF is located at a site of low-to-moderate seismic hazard, and is conventionally founded. The INL site, which is considered to have moderate seismic hazard is chosen for this case.

2. Case 2: GDNF is located at a site of high seismic hazard high hazard seismic site and is conventionally founded. The site of the Los Alamos National Laboratory is chosen for this case.
3. Case 3: GDNF is located at the same site as Case 2, but is base isolated.

Case 1 serves as the benchmark, where seismic isolation may (and may not) yield a significant economical benefit since the seismic hazard and the resultant demands on the SSCs are relatively low. Cases 2 and 3 present two options decision makers should consider if the GDNF of Case 1 is moved to a site of higher seismic hazard. For Case 2, the capacities of the SSCs would have to be strengthened, and the facility operator would have to demonstrate the seismic robustness of some of the equipment through rigorous qualification. For Case 3, the costs of strengthening and qualification can be avoided by seismically isolating the structure.

2. DESCRIPTION OF THE FACILITY

2.1 Structures, systems and components

2.1.1 Building and site description

The generic Department of Energy nuclear facility (GDNF) is located at the Idaho National Laboratory (INL) in Idaho Falls, ID. The facility is assumed to handle radiological materials (or materials at risk, MAR) and its structure, systems and components are designed to confine these materials in the event of an internal failure.

The GDNF building is a two-story structure composed of reinforced concrete and structural steel. The building is surface founded on a 4 ft. to 6.5 ft. thick basemat. The thickness of the reinforced concrete building walls ranges from 1 ft. to 3 ft. The building measures 75 ft. x 160 ft. in plan and is about 60 ft. tall at its highest point.

The INL site is mainly composed of alternating layers of alluvium and basaltic rock. The shear-wave velocity of the soil ranges from about 700 ft./sec to 1500 ft./sec, which is low for the site of a nuclear facility in the United States. Since the purpose of this study is to characterize costs and benefits, and to provide a framework for making risk-based decisions, the GDNF is founded on soft rock as characterized by soil at the boundary of Site Class B and Site Class C per ASCE/SEI Standard 7-10 (ASCE 2010). Soil-structure interaction analysis is not performed.

2.1.2 Systems analysis: event tree and fault tree

Safety-related nuclear facilities in the DOE complex have diverse functions and vary in terms of their size, properties and contents. The DOE complex includes nuclear structures that store spent fuel and radioactive materials, and large pools and tanks. Given this diversity, it is not possible choose SSCs for this study that are representative of all DOE structures. For this reason, and to avoid specificity, the systems and components in the GDNF facility are not used in this study. Instead, systems and components that are generic to safety-related nuclear structures are used to populate the facility.

A single system is chosen for risk assessment in this study. This system is intended to confine a loss of MAR to inside the structure. The event tree for this system is illustrated Figure 2-1, which shows that MAR may leak from the building if the system fails due to a seismic event.

The hypothetical fault tree for this system is presented in Figure 2-2. There are three key component categories in the fault tree: confinement, mechanical, and electrical. There are a total of eight components in these three categories, as listed in Table 2-1. The components are located in the GDNF on the basis of their function: see Figure 2-3. They are chosen from the EPRI “Seismic probabilistic risk assessment guide” (EPRI 2013), which also presents recommended fragilities. Here, structure (component 6) is assumed to be framing that surrounds the pressure vessel.

The fault tree is simplistic and important interactions between mechanical and electrical systems, and electrical systems and active confinement (HVAC) are not considered. The AND and OR gates in Figure 2-2 describe the assumed path (and resistance) to loss of material. The system is assumed to have failed if (1) confinement is lost, (2) mechanical components fail, or (3) electrical components fail. Failure of the isolation system might also lead to a loss of MAR, and this is characterized in Section 3.5.

Table 2-1 identifies the demand parameter that most influences the behavior of each SSC and the corresponding frequency range of interest.

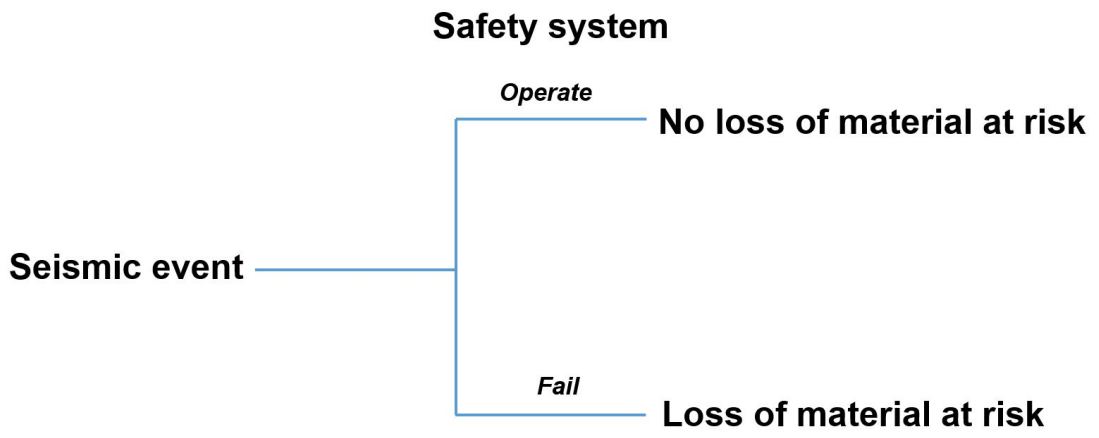

Figure 2-1: Event tree for the safety system considered for risk assessment

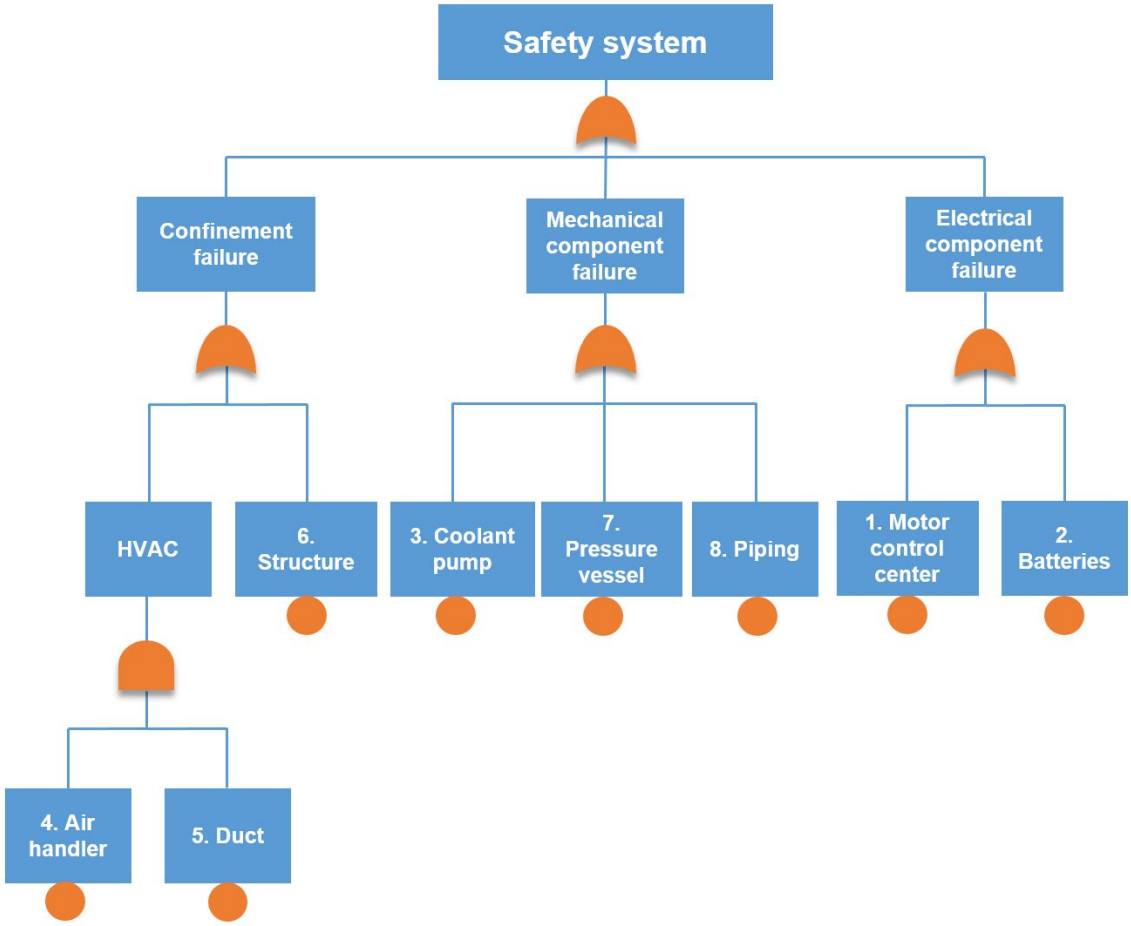

Figure 2-2: Fault tree for the safety system considered for risk assessment

Table 2-1: List of components, their locations and the corresponding frequency ranges

Component	Frequency range (Hz)	Demand from in-structure response spectra
1. Motor control center (MCC)	3-10	Average S_a [1] over frequency range (column 2)
2. Battery	10-15	Average S_a over frequency range
3. Coolant pump	7-10	Average S_a over frequency range
4. Air handler	10-20	Average S_a over frequency range
5. HVAC duct	2-20	Peak S_a over frequency range
6. Structure (around vessel)	5-10	Average S_a over frequency range
7. Pressure vessel	10-33	Average S_a over frequency range
8. Piping	4-40	Maximum of peak S_a over frequency range at all nodes

1. S_a denotes spectral acceleration

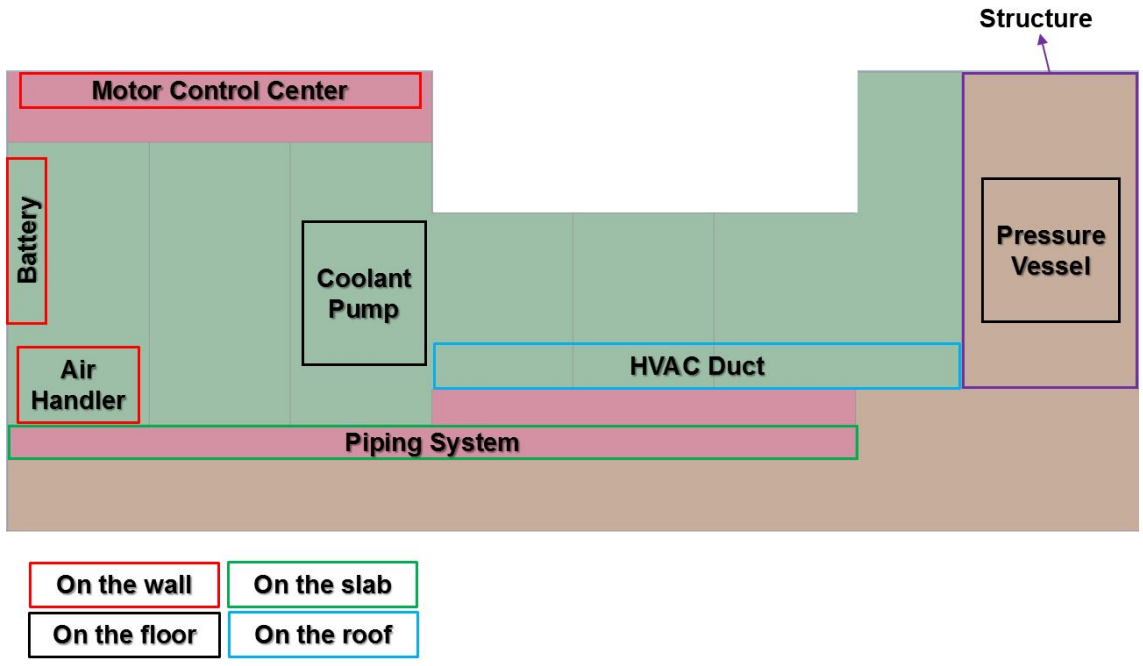

Figure 2-3: Plan view of GDNF identifying the assumed locations of components

2.2 Seismic hazard calculations and ground motion selection and scaling

The risk calculations and cost estimates performed for the three cases listed in Section 1.2 involve two sites: the Idaho National Laboratory (INL) in Idaho Falls, ID and the Los Alamos National Laboratory (LANL) in Los Alamos, NM. Seismic hazard data were developed using the USGS website (http://earthquake.usgs.gov/designmaps /us/application.php, accessed on June 1, 2016). The soil conditions at the INL and LANL sites are assumed to be identical and are characterized by the boundary between site classes B and C (ASCE 2010) for the purpose of calculating seismic hazard. Acceleration response spectra corresponding to a mean annual frequency of exceedance (MAFE) of 10^{-4} are generated for the two sites, and these spectra are used to represent design basis earthquake (DBE) shaking. The USGS hazard calculator (http://earthquake.usgs.gov/designmaps/us/application.php) is used for this purpose. Ground motions are then generated to be consistent with these spectra for nonlinear response-history analysis of the building at each site.

Design basis earthquake ground motions for nuclear facilities (ASCE 2005, USNRC 2007) are routinely presented as acceleration response spectra calculated as the product of a scalar design factor and uniform hazard response spectra. The design factor is used to enable a deterministic design to achieve target performance goals, which vary as a function of seismic design category: see ASCE 43-05 (ASCE 2005) for details. Herein, the design factor is not used because risk (or performance measured by a mean annual frequency of unacceptable performance) is calculated explicitly. Design basis ground motions are developed on the basis of uniform hazard spectra only.

The horizontal spectra for the INL and LANL sites are presented in Figure 2-4 in linear and logarithmic scales. The vertical spectra are generated by amplitude scaling the horizontal spectra using the V/H relationship recommended by Bozorgnia and Campbell (2004), which is presented in Figure 2-5.

Figure 2-6 presents results of the seismic hazard deaggregation for the two sites and two periods: 0.1 second that is assumed to be representative of the conventionally founded building and 2 seconds that is assumed to be representative of the isolated building. The deaggregation tool provided by the USGS (USGS, 2008) was used for the calculations. The modal magnitude-distance-epsilon triples (M, r, ε) for the two sites and the two periods are:

INL, ID, 0.1 second: 6.2, 7.9 km (4.9 miles), 0.31

INL, ID, 2 seconds: 6.8, 14.6 km (9.1 miles), 0.61

LANL, NM, 0.1 second: 6.8, 4.8 km (3.0 miles), 0.02

LANL, NM, 2 seconds: 6.8, 4.8 km (3.0 miles), 0.08

Ground motion time series are generated to be compatible with the spectra of Figure 2-4. The seed motions are taken from earthquake recordings. Thirty sets of three-component ground motions are generated for the two sites in two steps: 1) select seed motions based on the 2-second (M, r) pairs for each site, 2) match the seed motions to the target spectrum using a time-domain procedure, and 3) amplitude scale the two horizontal components in each set by factors to provide maximum direction-minimum direction (max-min) ground motions that recover the geometric mean.

The controlling (M, r) pairs at a period of 2 seconds for INL and LANL at a return period of approximately 10,000 years are (6.8, 14.6 km) and (6.8, 4.8 km), respectively. The controlling pairs at 0.1 second are not substantially different. Seed ground motions are selected from the PEER database (PEER

2011) for each site for these pairs. (The controlling pairs at 0.1 second are not substantially different and so additional seed motions are not mined from the PEER database.) Information is presented in Table 2-2 and Table 2-3, for the INL and LANL sites, respectively. The seed ground motions were matched to the target spectra using the wavelet-based procedure of RSPMatch2005 (Hancock et al. 2006), one component at a time.

Section 2.6.2 of ASCE 4-16 (ASCE 2016) writes that motions used for analysis of nuclear structures shall be statistically independent, with a mean correlation in a set being no greater than 0.16 and a maximum correlation of 0.3. These rules are based in part on the studies of Hadjian (1981) and Huang et al. (2011c, 2016), noting that Huang et al. show that the exceedance probability for 0.3 of as-recorded motions is about 10%. The correlation coefficients of the scaled motions are presented in Table 2.2-3. In this table, suffix 1 and suffix 2 correspond to the two horizontal components, and suffix 3 corresponds to the vertical component. The mean (average) correlation in each set is less than 0.16. The maximum correlation in two of the six sets is greater than 0.3, but there is only one exceedance per set. The ground motions comply with the rules of ASCE 4-16, with the exception of two values (out of 180) greater than 0.3. The ground motions are consistent with the recent studies of Huang et al. (2011c, 2016).

The spectrum-consistent ground motions were then scaled to maximum and minimum directions to reflect the differences in recorded pairs of horizontal motions (Huang et al. 2008a, 2009b). Amplitude scale factors F_h and $1/F_h$ were applied to the two horizontal components in each set, and these were selected by a Latin Hypercube Procedure from a lognormal distribution with a mean, θ, of 0.3 and a logarithmic standard deviation, β, of 0.13 (Huang et al. 2009b). The vertical components were similarly scaled by a factor F_v with a mean of 0.10 and a logarithmic standard deviation of 0.18. The scale factors are reported in Table 2-5. Figure 2-7 and Figure 2-8 present acceleration spectra of 5% damping for the Idaho Falls and Los Alamos sites, respectively. Each figure presents information for the spectrum-matched and max-min motions. The target horizontal spectra are geometric mean spectra.

Data are presented in this section for vertical ground motions for completeness. These ground motions were not input to the numerical models for calculating demand and risk because the available fragility functions are suitable only for characterizing the effects of *horizontal* shaking on structures, systems and components. It is anticipated that isolators would be designed *not* to amplify vertical shaking effects and the addition of an isolation system will not increase the vulnerability of structures, systems and components in the vertical direction. This assumption could be verified at a later time, using the vertical ground motions presented here, once fragility functions for shaking in the vertical direction become available.

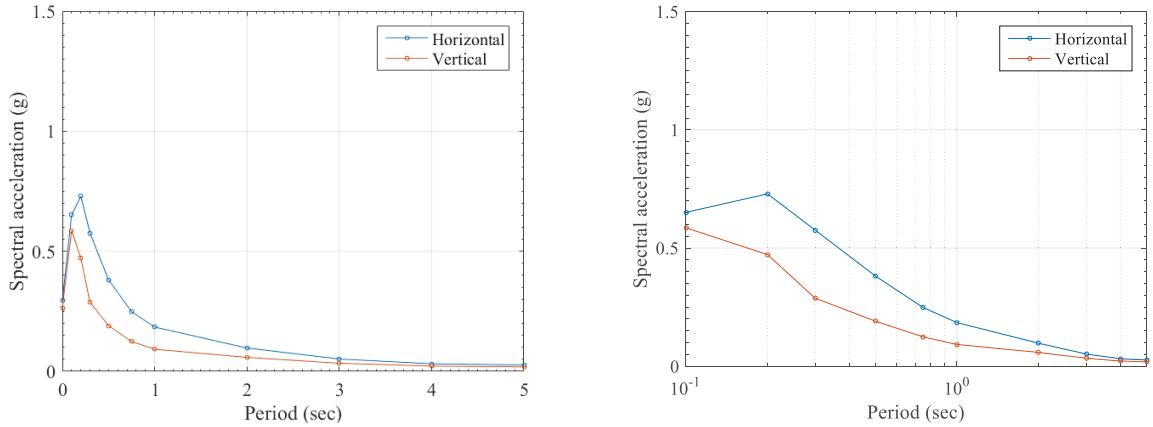

a. INL, linear scale

b. INL, log scale

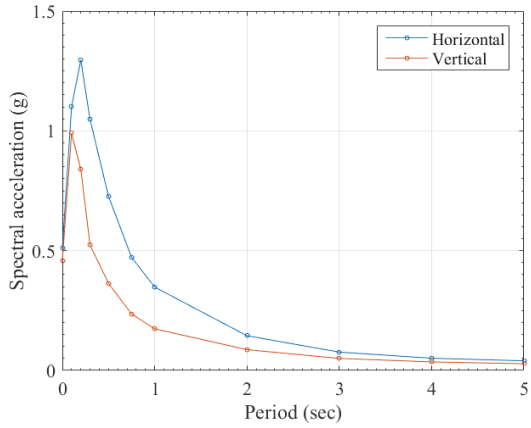

c. LANL, linear scale

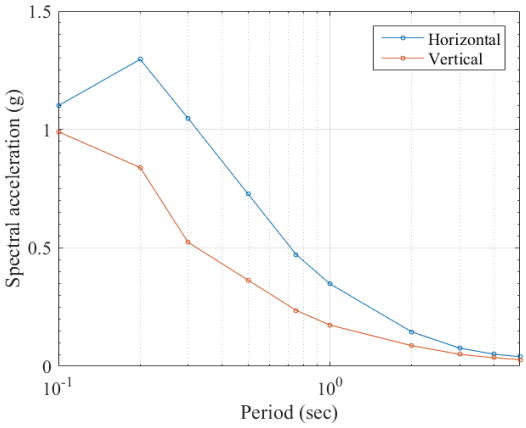

d. LANL, log scale

Figure 2-4: Horizontal and vertical acceleration spectra for a return period of 10,000 years and 5% damping: DBE shaking

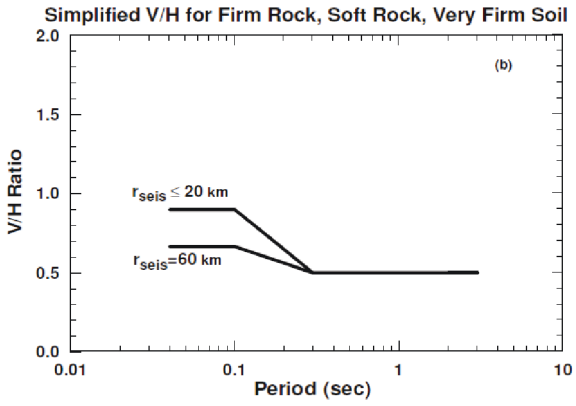

Figure 2-5: Vertical-to-horizontal spectral ratio (Bozorgnia and Campbell 2004)

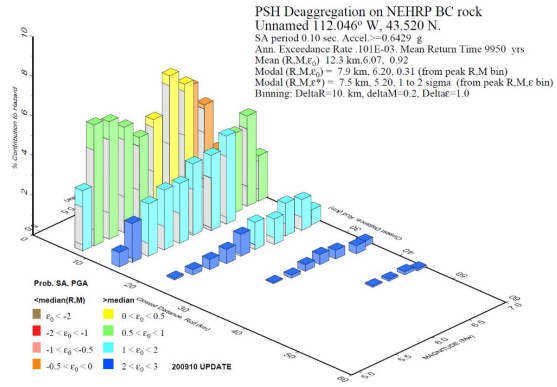

a. INL, 0.1 second

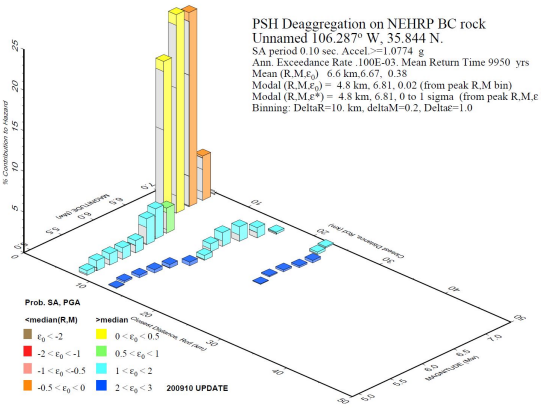

b. LANL, 0.1 second

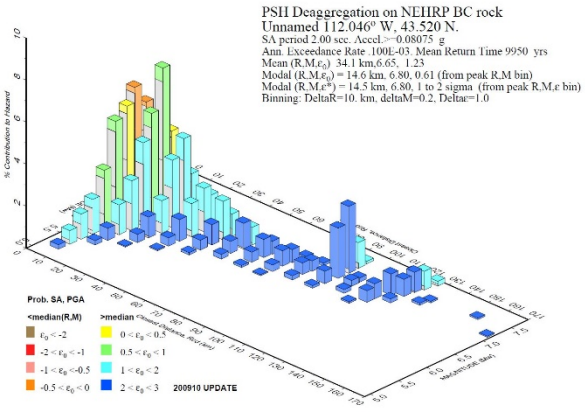

c. INL, 2 seconds

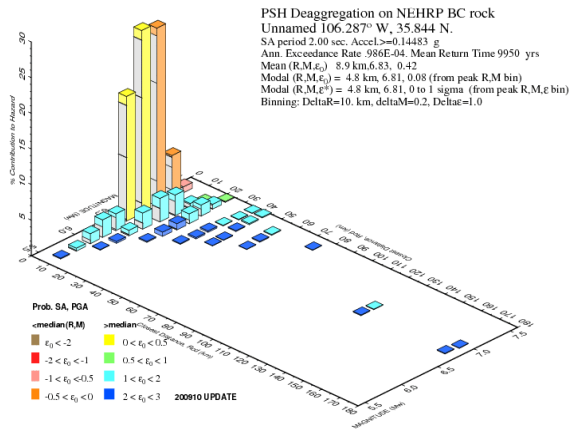

d. LANL, 2 seconds

Figure 2-6: Seismic hazard deaggregation data, INL and LANL, return period of 10,000 years: DBE shaking (USGS 2008)

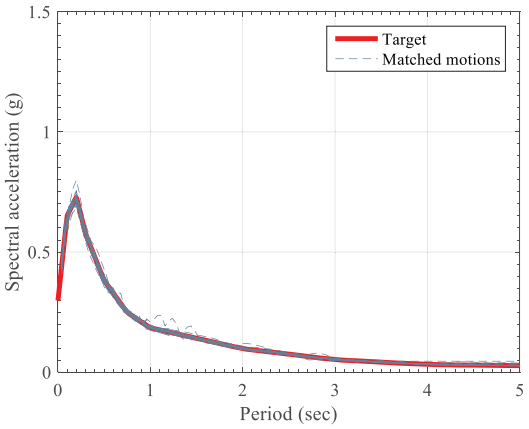

a. horizontal component 1, spectrum matched

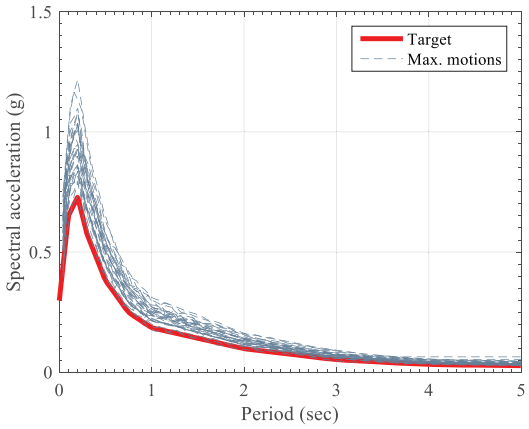

d. horizontal component 1, max direction

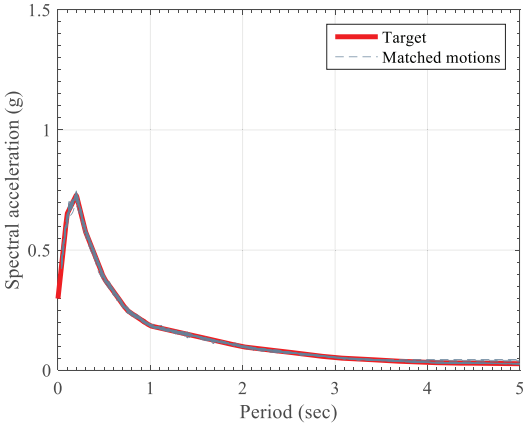

b. horizontal component 2, spectrum matched

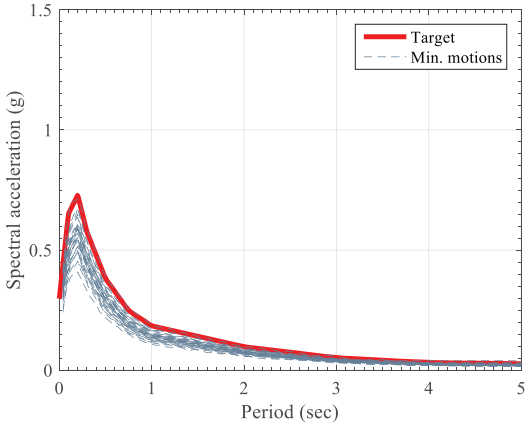

e. horizontal component 2, min direction

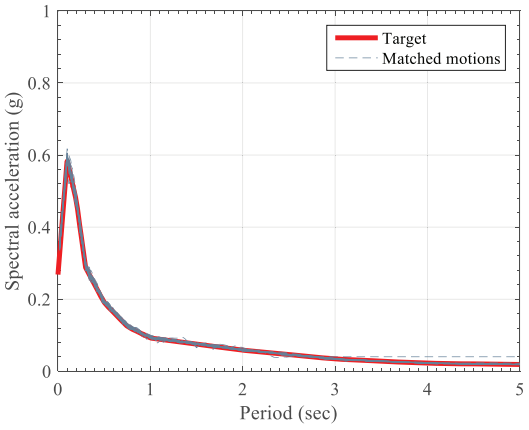

c. vertical component , spectrum-matched

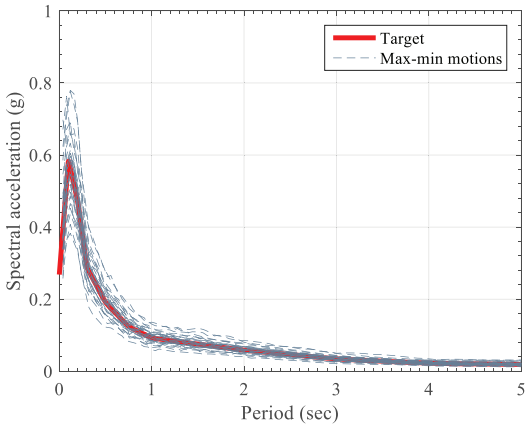

f. vertical component, max-min

Figure 2-7: Acceleration response spectra, INL, 5% damping: DBE shaking

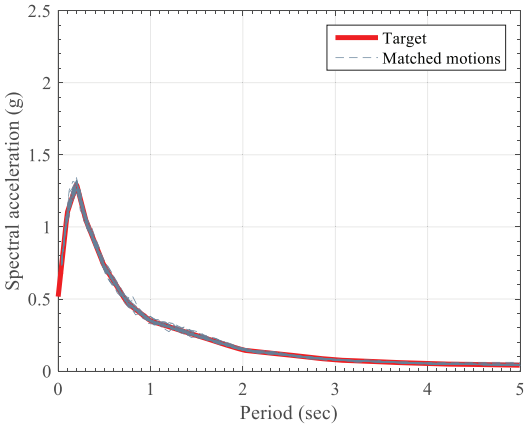

a. horizontal component 1, spectrum matched

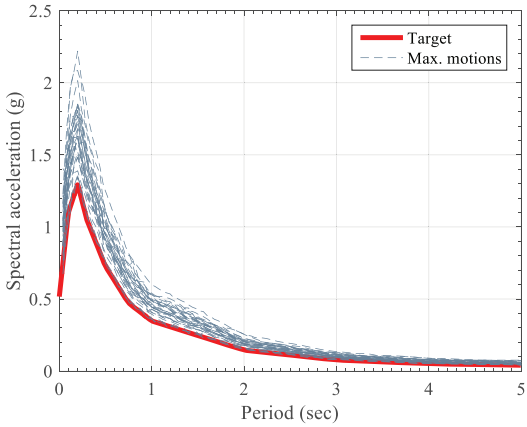

d. horizontal component 1, max direction

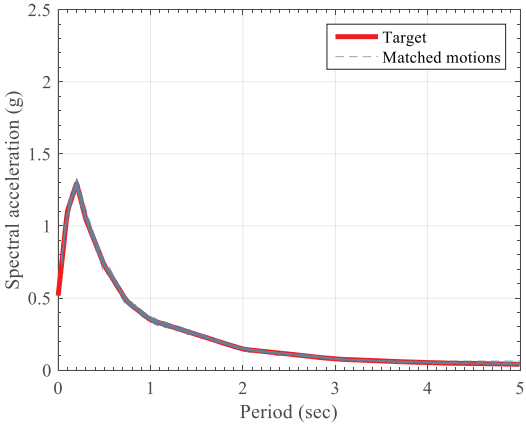

b. horizontal component 2, spectrum matched

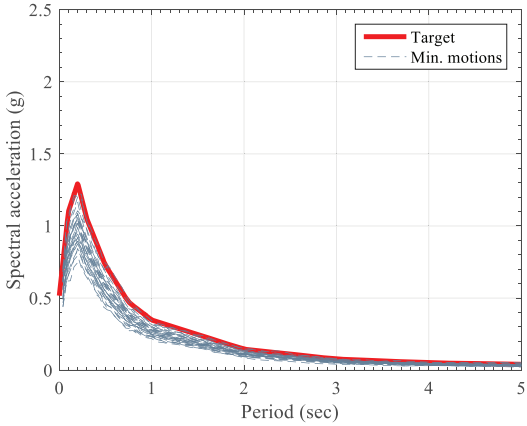

e. horizontal component 2, min direction

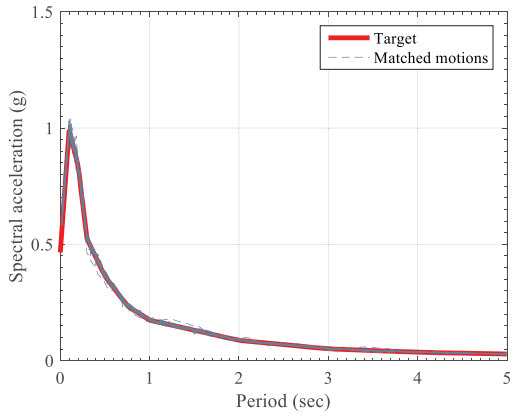

c. vertical component , spectrum-matched

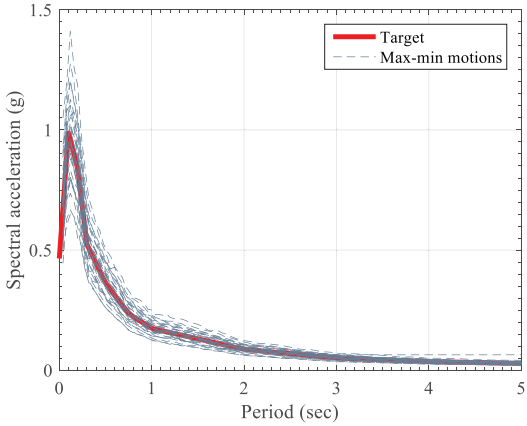

f. vertical component, max-min

Figure 2-8: Acceleration response spectra, LANL, 5% damping: DBE shaking

Table 2-2: Seed motions for the INL site

Earthquake	Year	Station Name	M[1]	r (km)[2]
Morgan Hill	1984	Anderson Dam (downstream)	6.19	3.26
Loma Prieta	1989	BRAN	6.93	10.72
Northridge	1994	Pacoima Kagel Canyon	6.69	7.26
Duzce, Turkey	1999	Lamont 1059	7.14	4.17
Duzce, Turkey	1999	Lamont 375	7.14	3.93
Duzce, Turkey	1999	IRIGM 496	7.14	4.21
Duzce, Turkey	1999	IRIGM 498	7.14	3.58
Chi-Chi, Taiwan	1999	TCU084	6.2	9.32
Chi-Chi, Taiwan	1999	TCU089	6.2	9.81
Chi-Chi, Taiwan	1999	CHY074	6.2	6.2
Chi-Chi, Taiwan	1999	TCU078	6.3	11.52
Tottori, Japan	2000	SMNH01	6.61	5.86
San Simeon, CA, USA	2003	Templeton-1-story hospital	6.52	6.22
Parkfield, CA, USA	2004	Parkfield-Donnalee	6	4.93
Parkfield, CA, USA	2004	Parkfield-Turkey Flat #1 (0M)	6	5.29
Parkfield, CA, USA	2004	Bear Valley Ranch	6	4.32
Parkfield, CA, USA	2004	Parkfield-Cholame 2E	6	4.08
Parkfield, CA, USA	2004	Parkfield-Cholame 4W	6	4.23
Parkfield, CA, USA	2004	Parkfield-Fault Zone 11	6	4
Parkfield, CA, USA	2004	Parkfield-Gold Hill 3W	6	5.41
Parkfield, CA, USA	2004	Parkfield-Stone Corral 2E	6	5.8
Parkfield, CA, USA	2004	Parkfield-Vineyard Cany 2E	6	4.46
Parkfield, CA, USA	2004	Parkfield-Gold Hill 4W	6	8.27
Parkfield, CA, USA	2004	Parkfield-Stone Corral 3E	6	8.08
L'Aquila, Italy	2009	Gran Sasso (Assergi)	6.3	6.4
Chuetsu-oki, Japan	2007	Nagaoka	6.8	16.27
Chuetsu-oki, Japan	2007	Tani Kozima Nagaoka	6.8	13.75
Iwate, Japan	2008	WITH 24	6.9	5.18
Iwate, Japan	2008	Mizusawaku Interior O ganecho	6.9	7.85
Big Bear	1992	Big Bear Lake-Civic Center	6.46	8.3

1. Moment magnitude
2. Smallest site-fault rupture distance

Table 2-3: Seed motions for the LANL site

Earthquake	Year	Station Name	M[1]	r (km)[2]
Morgan Hill	1984	Anderson Dam (Downstream)	6.19	3.26
Loma Prieta	1989	BRAN	6.93	10.72
Northridge	1994	Pacoima Kagel Canyon	6.69	7.26
Duzce, Turkey	1999	Lamont 1059	7.14	4.17
Duzce, Turkey	1999	Lamont 375	7.14	3.93
Duzce, Turkey	1999	IRIGM 496	7.14	4.21
Duzce, Turkey	1999	IRIGM 498	7.14	3.58
Duzce, Turkey	1999	IRIGM 487	7.14	2.65
Chi-Chi, Taiwan	1999	TCU084	6.2	9.32
Chi-Chi, Taiwan	1999	TCU089	6.2	9.81
Chi-Chi, Taiwan	1999	CHY074	6.2	6.2
Chi-Chi, Taiwan	1999	TCU078	6.3	11.52
San Simeon, CA, USA	2003	Templeton-1-story Hospital	6.52	6.22
Parkfield, CA, USA	2004	Parkfield-Donnalee	6	4.93
Parkfield, CA, USA	2004	Parkfield-Turkey Flat #1 (0M)	6	5.29
Parkfield, CA, USA	2004	Bear Valley Ranch	6	4.32
Parkfield, CA, USA	2004	Parkfield-Gold Hill 3E	6	6.3
Parkfield, CA, USA	2004	Parkfield-Gold Hill 3W	6	5.41
Parkfield, CA, USA	2004	Parkfield-Stone Corral 2E	6	5.8
Parkfield, CA, USA	2004	Parkfield-Vineyard Cany 2E	6	4.46
Parkfield, CA, USA	2004	Parkfield-Gold Hill 4W	6	8.27
Parkfield, CA, USA	2004	Parkfield-Stone Corral 3E	6	8.08
L'Aquila, Italy	2009	Gran Sasso (Assergi)	6.3	6.4
Chuetsu-oki, Japan	2007	Nagaoka	6.8	16.27
Chuetsu-oki, Japan	2007	Yoitamachi Yoita Nagaoka	6.8	16.1
Chuetsu-oki, Japan	2007	Tani Kozima Nagaoka	6.8	13.75
Iwate, Japan	2008	WITH 24	6.9	5.18
Iwate, Japan	2008	Mizusawaku Interior O ganecho	6.9	7.85
Big Bear	1992	Big Bear Lake-Civic Center	6.46	8.3
Christchurch, New Zealand	2011	LPCC	6.2	2.52

1. Moment magnitude

2. Smallest site-fault rupture distance

Table 2-4: Correlation coefficients

	INL			LANL		
Set[1]	ρ_{12}	ρ_{23}	ρ_{23}	ρ_{12}	ρ_{23}	ρ_{23}
1	0.139	0.133	0.142	0.148	0.132	0.175
2	0.211	0.076	0.011	0.232	0.088	0.031
3	0.165	0.093	0.046	0.233	0.072	0.047
4	0.294	0.406	0.171	0.276	0.351	0.203
5	0.139	0.023	0.023	0.155	0.016	0.015
6	0.199	0.219	0.222	0.193	0.206	0.231
7	0.247	0.208	0.208	0.260	0.200	0.269
8	0.107	0.025	0.088	0.231	0.173	0.185
9	0.200	0.198	0.144	0.120	0.026	0.016
10	0.124	0.072	0.109	0.209	0.247	0.137
11	0.115	0.007	0.047	0.067	0.042	0.120
12	0.089	0.290	0.242	0.147	0.015	0.055
13	0.101	0.003	0.078	0.104	0.025	0.081
14	0.255	0.063	0.196	0.276	0.010	0.196
15	0.022	0.039	0.024	0.029	0.046	0.035
16	0.042	0.106	0.227	0.040	0.133	0.238
17	0.006	0.021	0.006	0.113	0.063	0.040
18	0.029	0.035	0.009	0.159	0.061	0.033
19	0.157	0.042	0.105	0.044	0.090	0.025
20	0.137	0.060	0.013	0.235	0.001	0.023
21	0.025	0.068	0.039	0.088	0.027	0.013
22	0.235	0.045	0.072	0.138	0.031	0.015
23	0.159	0.014	0.077	0.031	0.050	0.154
24	0.027	0.083	0.023	0.138	0.019	0.010
25	0.060	0.039	0.151	0.164	0.199	0.246
26	0.106	0.012	0.002	0.283	0.052	0.030
27	0.261	0.035	0.032	0.073	0.071	0.068
28	0.043	0.094	0.045	0.071	0.105	0.104
29	0.048	0.092	0.110	0.149	0.030	0.133
30	0.155	0.036	0.155	0.086	0.053	0.296
Average	0.130	0.088	0.094	0.150	0.088	0.107
Maximum	0.294	0.406	0.242	0.283	0.351	0.296

1. Motions after spectrum matching from Tables 2-2 and 2-3.

Table 2-5: Amplitude scale factors for maximum-minimum motions

	INL			LANL		
Set[1]	F_h	$\frac{1}{F_h}$	F_v	F_h	$\frac{1}{F_h}$	F_v
1	1.27	0.79	0.97	1.26	0.79	1.04
2	1.62	0.62	1.20	1.22	0.82	1.06
3	1.37	0.73	0.82	1.23	0.81	0.93
4	1.42	0.71	1.26	1.39	0.72	0.87
5	1.32	0.76	0.92	1.41	0.71	1.12
6	1.35	0.74	1.13	1.41	0.71	1.33
7	1.25	0.80	0.84	1.72	0.58	0.88
8	1.68	0.59	1.04	1.11	0.90	0.91
9	1.09	0.92	1.43	1.16	0.86	0.83
10	1.43	0.70	0.98	1.08	0.92	1.40
11	1.12	0.89	1.12	1.17	0.85	0.70
12	1.07	0.94	1.15	1.34	0.75	0.72
13	1.30	0.77	1.00	1.47	0.68	1.19
14	1.23	0.81	1.08	1.30	0.77	1.24
15	1.24	0.81	0.79	1.14	0.87	1.01
16	1.38	0.72	1.38	1.36	0.74	1.15
17	1.47	0.68	0.87	1.21	0.83	1.03
18	1.19	0.84	0.89	1.53	0.65	0.86
19	1.40	0.72	1.29	1.19	0.84	0.96
20	1.20	0.83	1.03	1.48	0.68	0.81
21	1.47	0.68	0.95	1.60	0.63	0.98
22	1.31	0.76	0.66	1.45	0.69	0.77
23	1.50	0.66	1.18	1.31	0.77	0.92
24	1.14	0.88	0.90	1.57	0.64	1.26
25	1.28	0.78	1.09	1.04	0.97	1.06
26	1.55	0.64	1.01	1.28	0.78	1.08
27	1.16	0.87	1.06	1.32	0.76	1.11
28	1.17	0.86	0.72	1.37	0.73	1.17
29	0.99	1.01	0.93	1.25	0.80	0.97
30	1.34	0.75	0.85	1.02	0.98	0.99

1. Motions after spectral matching from Tables 2-2 and 2-3.

2.3 Numerical model of the building

As-built drawings of the building are used to construct the numerical model for simulations. These drawings are not included in this report. The basemat of the building is modified to have a uniform thickness of 6.5 ft. The finite element software LS-DYNA (LSTC 2013) was used to model the facility and perform nonlinear response-history analysis of the conventionally founded and base-isolated variants of the structure. The LS-DYNA model is described below.

Two finite element models of the facility were developed in the finite element code LS-DYNA: 1) the conventionally founded building, and 2) the isolated building (See Section 2.4). Figure 2-9a presents a schematic view of the LS-DYNA model, showing the global coordinate system (X, Y, Z) and representative dimensions. Figure 2-9b presents the finite element model of the 6ft thick basemat consisting of 368 eight-node solid elements. Figure 2-9c through Figure 2-9f present the finite element models of walls and roofs of the building built using four-node shell elements. A linear elastic material model is assigned to the shell and solid elements, and the material properties of concrete are used: Young's modulus, E, of 5.2×105 kip/ft^3, Poisson's ratio of 0.17, and mass density of 4.7×10^{-3} kip-s^2/ft^4.

The total dead load, including the basemat, is 21,280 kips and the assumed live load is 3,100 kips. The seismic (reactive) weight is taken as the dead load and one half of the live load 22,845 kips, per ASCE/SEI 7-10 (ASCE 2010). The building responds dynamically in many modes. Seven hundred and ten modes are needed to capture 90% of the mass in the three orthogonal directions. Table 2-6 presents summary information on the modal properties of the LS-DYNA model, including the seven modes that contribute most significantly to the modal effect mass (MEM) in each orthogonal direction. Modes are listed in a descending order of their contribution to MEM. In the X direction (see Figure 2-9 for directions), modes 5, 6, 9, 7, 12, 16, and 4 contribute 72% of the mass; in the Y direction, modes 4, 3, 5, 11, 7, 20, and 1 contribute 76% of the mass; and in the Z direction, modes 40, 18, 93, 26, 38, 29, and 43 contribute 38% of the mass.

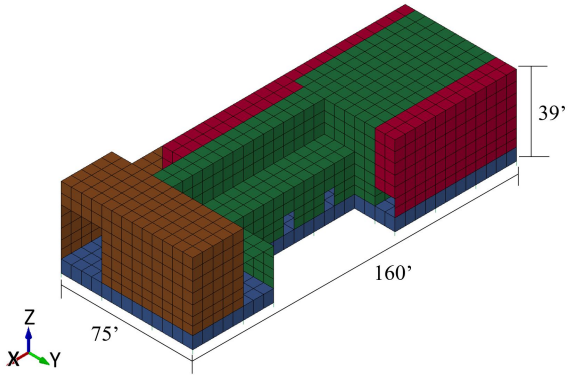

a. Schematic view

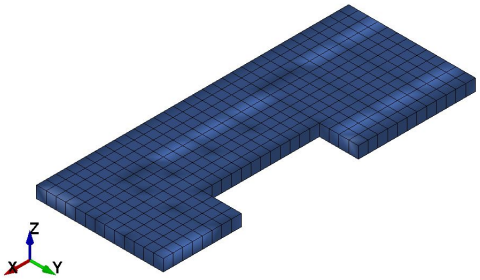

b. basemat (solid elements)

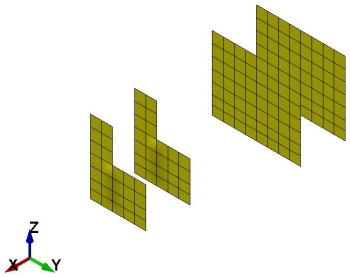

c. walls (shell elements)

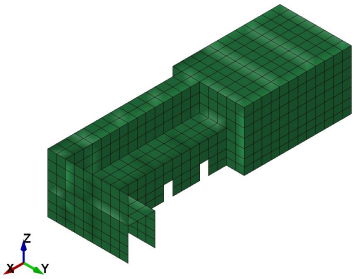

d. cell walls and roof (shell elements)

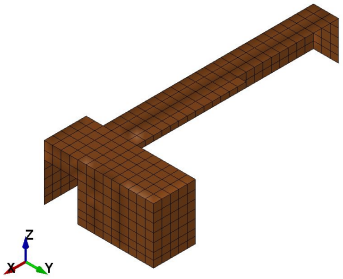

e. corridor walls, slab and roof (shell elements)

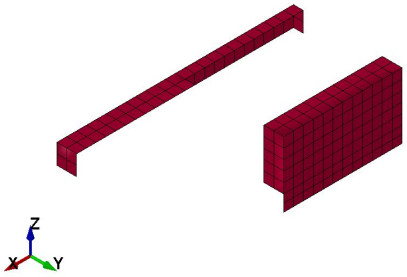

f. transfer corridor walls and roof (shell elements)

Figure 2-9: LS-DYNA model of the IWTU

Table 2-6: Modal properties of the LS-DYNA model, ordered by modal effective mass

X direction			Y direction			Z direction		
Mode	Period (sec)	MEM (%)	Mode	Period (sec)	MEM (%)	Mode	Period (sec)	MEM (%)
5	0.047	23.8	4	0.050	40.0	40	0.021	11.2
6	0.042	14.4	3	0.051	19.1	18	0.028	6.3
9	0.037	10.3	5	0.047	8.3	93	0.015	5.0
7	0.042	6.6	11	0.036	3.9	26	0.024	4.8
12	0.035	6.1	7	0.042	2.0	38	0.021	4.2
16	0.030	5.8	20	0.026	1.6	29	0.024	3.8
4	0.050	4.5	1	0.099	1.6	43	0.020	2.8

2.4 Design and modeling of the isolation system

The seismic isolation system was designed per the provisions of ASCE 4-16 (ASCE 2016) using an iterative process, and equations and assumptions that are presented in Constantinou et al. (2007) and McVitty and Constantinou (2015). The steps in the design process are not presented here but the end product is: number of isolators, size of isolators. The lead-rubber (LR) isolator is chosen for this study: one of the three types of isolators permitted per ASCE 4-16. This type of isolator is circular and is composed of alternating layers of natural rubber and steel shim plates. A central, cylindrical lead plug in each bearing dissipates energy.

Chapter 12 of ASCE 4-16 provides mandatory language for the analysis and design of a seismic isolation system and for testing of prototype and production isolators. Analysis is performed for design basis earthquake (DBE) shaking (see Section 2.2) and for 150% of DBE shaking. Results of analysis for 150% DBE shaking are used to calculate horizontal displacement and axial force demands on isolators for prototype testing. Figure 2-10 identifies the location of the 38 LR isolators used to protect the GDNF.

Figure 2-10: Plan layout of isolators for the GDNF

The 38 LR isolators are modeled with the material *MAT_SEISMIC_ISOLATOR (197) available in LS-DYNA (LSTC, 2013). Analysis is performed for both the LANL and INL sites for completeness, noting that isolation is only being considered for the LANL site in this study.

The product of the iterative analysis is one size of isolator: 31 inches in diameter, central lead plug of 6 inches in diameter, 25 layers of 0.42-inch thick rubber, 24 0.2-inch thick shim plates, 2 1.25-inch diameter end plates, and 2 1.25-inch thick flange plates, for a total bearing height of 20 inches. The isolator design and locations were not optimized, nor was the framing above the bearing adjusted to best utilize the isolation system: activities that would have maximized the efficiency of the isolation system, minimized both lateral displacements in both horizontal directions, and reduced the risk of failure of the isolation system. The rated displacement capacity of this isolator, manufactured by Dynamic Isolation System, in Sparks, NV, is 20 inches, and the corresponding maximum axial force is 1100 kips.

The sizing of the LR isolator is controlled by the results of analysis for 150% DBE shaking. The 90th percentile lateral displacement of the isolation system for the LANL (INL) site is 14 (9) inches: much less than the rated capacity of 20 inches. The 90th percentile compressive load on the isolator (maximum of all 38 isolators) at the LANL (INL) site is 913 (862) kips: much less than the rated capacity at 20 inches lateral displacement of 1100 kips.

3. REDUCING RISK USING SEISMIC ISOLATION

3.1 Introduction

Seismic probabilistic risk assessment (SPRA) is used to compute the mean annual frequency of unacceptable performance, such as core damage and large early radiation release for nuclear power plants (NPPs). The SPRA methodology used in this study is the methodology proposed by Huang et al. (2008b, 2011a, 2011b), which was developed to accommodate nonlinear elements in the soil-structure system, including nonlinear seismic isolators. This methodology shares many of the basic features of the Seismic Safety Margin method developed at Lawrence Livermore National Laboratory (Smith et al., 1981).

Figure 3-1 presents the five-step Huang SPRA methodology. Step 1 involves a plant system analysis. Event trees and fault trees leading to an accident associated with unacceptable performance (e.g., core damage) are developed, by-and-large consistent with current practice. Fragility curves for the components contributing to the accident sequence are developed, with demands local to each component (e.g., story drift for a shear wall, spectral acceleration at 5 Hz at the point of attachment for a motor control center), rather than the traditional practice of indirectly linking local demands to a ground motion parameter such as peak horizontal ground acceleration in the free field via in-structure seismic demand estimates derived from stand-alone hazard-compatible structural response analyses.

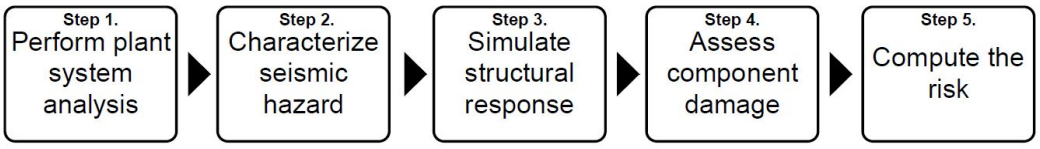

Figure 3-1: Huang et al. SPRA methodology (Huang et al. 2008b, 2011a)

Step 2 involves probabilistic seismic hazard analysis (PSHA), which is routinely performed for Department of Energy (DOE) and Nuclear Regulatory Commission (NRC) projects. Hazard calculations are site specific, and can be performed for surface free field or free field at some horizon below the ground surface. Seismic hazard curves, which are a product of PSHA, are generated for user-specified fundamental periods, which might be, for example: a) the fundamental period of the soil-structure system estimated for design basis earthquake shaking, b) the fundamental translational period of the nuclear power plant superstructure, and c) the first translation period of an isolated nuclear power plant, based on expected displacements at design basis earthquake shaking. In Huang's methodology, the hazard curve is split into multiple intervals for response-history and risk calculations, where the intervals span the range of interest in risk space (zero probability of failure through 100% probability of failure). (Here, six intervals of spectral acceleration are assumed, two less than the eight assumed in the implementation presented in FEMA P-58 (FEMA, 2012)). Each interval has a mid-point spectral acceleration ($S_{a,i}$ for the *i*th interval) and a mean annual frequency of occurrence ($\lambda\Delta_i$). Figure 3-2 illustrates the division of a seismic hazard curve into eight intervals, each with a mid-point spectral acceleration of $S_{a,i} = e_i$ and a corresponding mean annual frequency of exceedance. Three-component ground motion acceleration time series are scaled to each value of e_i, and these are used for response-history analysis in the next step. (Note that these time series could be input to a 3D soil-structure model or a 3D model of a structure if soil-structure-interaction effects are negligible.) Here, six intensities are assumed sufficient to calculate a robust estimate of demand and risk.

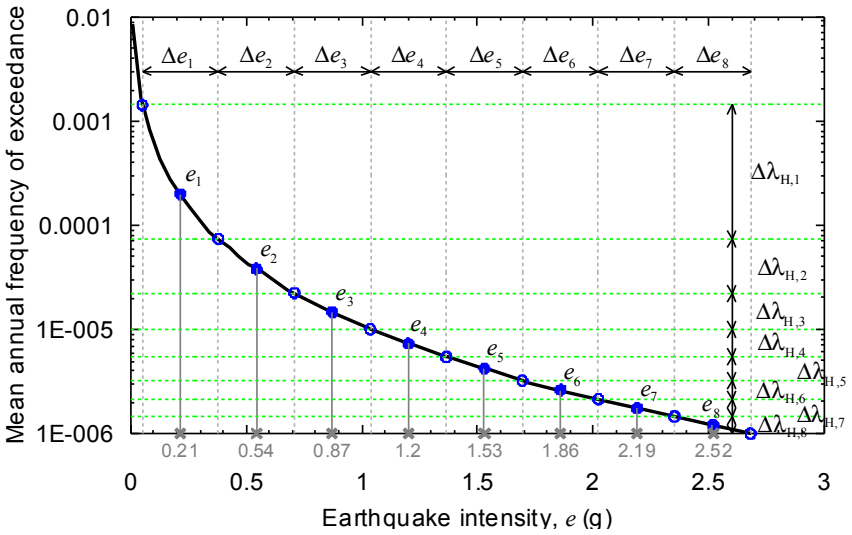

Figure 3-2: Seismic hazard curve, midpoint spectral accelerations, and mean annual frequencies of occurrence (Huang et al. 2011a)

The ground motions of Step 2 are used in Step 3 to perform tens of nonlinear response-history analyses of the 3D model of the soil-structure or structural system. Component demands at each of the intensities of shaking are then described by mean values, logarithmic standard deviations and cross correlation coefficients. Using a procedure developed by Yang et al. (2009) and implemented in FEMA P-58, the tens of values of demand are replaced by 100s to 1000s of realizations of demand for Monte Carlo simulations. Step 4 uses the realizations of Step 3 and the fragility functions of Step 1 for systems analysis. The product of this analysis, for each of the intensities of shaking, is a conditional probability of failure. In step 5, the conditional probability of failure for each (midpoint) intensity of shaking, $S_{a,i}$, is multiplied by the corresponding mean annual frequency of occurrence of the shaking in the interval, $\Delta\lambda_i$, to calculate a contribution to the total risk.

3.2 Hazard analysis and ground motions for risk calculations

Hazard analysis is performed for the two sites described in Section 2, namely, the Idaho National Laboratory (INL) and the Los Alamos National Laboratory (LANL). Seismic hazard curves for these sites and periods of 0.1 second (representative of the conventionally founded facility) and 2 seconds (representative of the isolated facility) are presented in Figure 3-3. The curves were generated for the return period of 10,000 years and a shear-wave velocity in the upper 100 ft. (30 m) of the soil column of 2500 ft./sec (760 m/sec): the boundary between Site Class B and C in ASCE 7-10.

The hazard curves of Figure 3-3 are divided to 6 intervals of ground motion intensity, all multiples of design basis earthquake (DBE) shaking: 0.5DBE, DBE, 1.5DBE, 2DBE, 2.5DBE, and 3DBE. The midpoint spectral accelerations and the corresponding mean annual frequencies of occurrence are listed in Table 3-1.

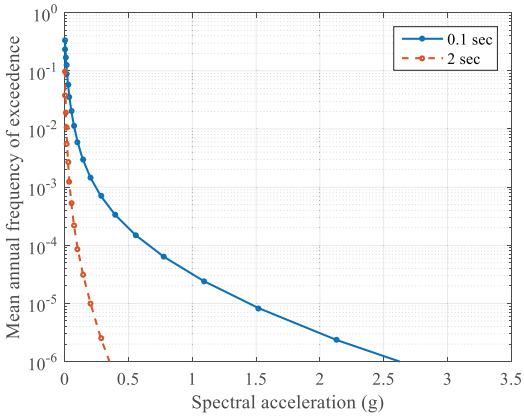

a. INL

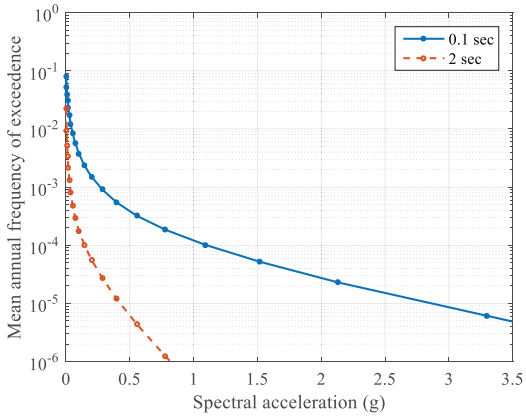

b. LANL

Figure 3-3: Seismic hazard curves at 0.1 second and 2.0 seconds for INL and LANL

Table 3-1: Midpoint spectral accelerations, $S_{a,i}$, and mean annual frequencies of occurrence, $\Delta\lambda_i$

a. INL

i	T = 0.1 sec		T = 2 sec	
	$S_{a,i}$ (g)	$\Delta\lambda_i$	$S_{a,i}$ (g)	$\Delta\lambda_i$
1	0.33	2.16E-03	0.05	3.19E-03
2	0.65	1.54E-04	0.10	1.68E-04
3	0.98	3.53E-05	0.15	3.55E-05
4	1.30	1.19E-05	0.20	1.12E-05
5	1.63	4.78E-06	0.24	4.28E-06
6	1.95	2.32E-06	0.29	1.69E-06

b. LANL

i	T = 0.1 sec		T = 2 sec	
	$S_{a,i}$ (g)	$\Delta\lambda_i$	$S_{a,i}$ (g)	$\Delta\lambda_i$
1	0.55	7.94E-04	0.07	6.97E-04
2	1.10	1.04E-04	0.15	9.20E-05
3	1.65	3.50E-05	0.22	3.33E-05
4	2.20	1.47E-05	0.29	1.55E-05
5	2.75	7.21E-06	0.36	8.28E-06
6	3.30	3.81E-06	0.44	4.37E-06

For response-history analysis, the pairs of horizontal ground motions of Section 2.2 are amplitude scaled by the six factors, 0.5 through 3. The orientation of the maximum component was randomly assigned to either the X or Y direction of Figure 2-9. The product of this exercise is 30 sets of maximum-minimum ground motions at six intensities of ground shaking. The results of analysis using the 30 DBE ground motions is used in the following section to generate fragility functions that are used for risk calculations. Only horizontal pairs of motions are used for analysis because the fragility curves used below address horizontal shaking only.

3.3 Generation of fragility functions for SSCs

Fragility curves must be developed to enable calculations of risk (or mean annual frequency of unacceptable performance). The cumulative lognormal distribution is widely used for describing fragility curves. The variable used to characterize fragility can vary by application, has traditionally been peak ground acceleration, but should be a demand parameter that best characterizes the response of the component (e.g., floor spectral acceleration for some equipment, story drift for reinforced concrete shear walls). Fragility curves can be defined using a double lognormal model, which is a cumulative lognormal distribution with an uncertain median value, as presented in Eq. (3-1):

$$P_f\left(a\right) = \Phi\left[\frac{\ln\left(a/\overline{a}\right)}{\beta_r}\right] \tag{3-1}$$

where $P_f\left(a\right)$ is the probability of failure of the component at a demand of *a*. The aleatory variability (or randomness) is described by the logarithmic standard deviation β_r. The aleatory variability is inherent in the variable *a*, and cannot be reduced. Parameter $\overline{a}$ is the median (50%-ile) of the fragility and is used to characterize the capacity of the component, which follows cumulative lognormal distribution as follows:

$$\overline{a} = \hat{a} \cdot e^{-\Phi^{-1}(Q)\cdot\beta_u} \tag{3-2}$$

where $\hat{a}$ is the median value of the capacity of the component; β_u is the logarithmic standard deviation in the capacity of the component that describes the epistemic uncertainty associated with a lack of knowledge (and can be reduced), and *Q* is the probability of exceedance associated with a given capacity $\overline{a}$.

In this study, the assumed accident involves the eight components listed in Table 2-1. Response-based fragility curves are developed for these components. The fragility curve used here is the *mean* curve proposed by Reed and Kennedy (1994), which is the weighted average of all possible curves with different median values, $\overline{a}$. The mean fragility curve has a median defined by the median capacity, $\hat{a}$, and a composite logarithmic standard deviation, β_c, given by:

$$P_f\left(a\right) = \Phi\left[\frac{\ln\left(a/\hat{a}\right)}{\beta_C}\right] \tag{3-3}$$

where the composite logarithmic standard deviation, β_c, is given by:

$$\beta_c = \sqrt{\beta_u^{\,2} + \beta_r^{\,2}} \tag{3-4}$$

Values for the parameters $\hat{a}$, β_u, and β_r define a fragility curve. The value of *a* associated with a 95% confidence of a 5% probability of failure is defined as the high-confidence-of-low-probability (HCLPF) capacity. Solving for *a* in Eq. (3-1) with P_f = 5% and assuming *Q* = 95% in Eq. (3-2) leads to a HCLPF capacity per Eq. (3-4):

$$HCLPF = \hat{a} \cdot e^{-1.65(\beta_r+\beta_u)} \tag{3-5}$$

For this study, the HCLPF capacities for the eight components are attached to the median responses of the conventionally founded structure calculated by analysis using the 30 DBE ground motions. The chosen response quantity varies by component per Table 2-1. The responses, which are all related to

spectral acceleration for the components selected here, are calculated at the locations shown in Figure 2-3. Responses are calculated for a damping ratio of 2% of critical. Table 3-2 presents the median responses of each component in the (horizontal) X and Y directions (see Figure 2-9) for the sample INL and LANL sites of the GDNF. The greater of the values in the X and Y directions is used to develop the fragility curve for the component. The median value, $\hat{a}$, of the fragility curve can be back calculated from Eq. (3-5) given the HCLPF capacity and values for β_u and β_r.

EPRI (2003) proposed values of β_u and β_r for peak ground acceleration- (PGA-) based fragility curves for components of nuclear structures. The values of β_u and β_r for PGA-based fragility curves include uncertainty in structure response. The risk calculations performed in this study use fragility curves characterized using local responses (e.g., average floor spectrum acceleration at the point of attachment) because demands on components are calculated directly by response-history analysis. However, in this study, the values of β_u and β_r in EPRI (2003) are used to calculate β_c per Eq. (3-4) because a) no better values are available, and b) the use of these values should not bias the relative risks in the conventionally founded and isolated GDNF. Values for $\hat{a}$, β_u, β_r, and β_c are presented in Table 3-3. Figures 3-4 and 3-5 present the mean fragility curve and values of the parameters that define the distribution, for each component listed in Table 2-1 for the INL and LANL sites, respectively.

Some of the median capacities listed in Table 3-3 are high and result from a) the calculation procedure used (which is robust), and b) the assumed point of attachment of the component and the use of maximum (X or Y) demand to calculate the required capacity. A project-specific design of a conventionally founded GDNF would likely reposition some of the components to avoid these high demands, for a relatively low level of earthquake shaking.

Table 3-2: Median DBE responses and HCLPF values

Component	INL			LANL		
	Median response-X (g)	**Median response-Y (g)**	**HCLPF**	**Median response-X (g)**	**Median response-Y (g)**	**HCLPF**
1. DC MCC	0.92	4.48	4.48	1.64	7.80	7.80
2. Battery	1.23	0.92	1.23	2.07	1.51	2.07
3. Coolant pump	0.89	0.89	0.89	1.49	1.47	1.49
4. Air handler	0.86	0.97	0.97	1.45	1.63	1.63
5. HVAC duct	2.25	7.48	7.48	3.63	12.4	12.4
6. Structure	0.98	1.01	1.01	1.71	1.65	1.71
7. Pressure vessel	0.59	0.59	0.59	1.02	0.99	1.02
8. Piping	2.11	7.69	7.69	3.41	12.7	12.7

Table 3-3: Fragility parameters

Component	$\hat{a}$		β_u	β_r	β_c
	INL	LANL			
1. DC MCC	14.5	28.3	0.30	0.35	0.46
2. Battery	4.0	7.4	0.30	0.35	0.46
3. Coolant pump	3.1	6.4	0.30	0.40	0.50
4. Air handler	3.4	6.3	0.30	0.40	0.50
5. HVAC duct	33.8	65.0	0.35	0.50	0.61
6. Structure	3.3	6.6	0.30	0.35	0.46
7. Pressure vessel	1.9	3.9	0.30	0.35	0.46
8. Piping	32.0	62.3	0.30	0.50	0.58

3.4 Risk calculations for SSCs

The calculation of the mean annual frequency of unacceptable performance involves nonlinear response-history analysis of the numerical models of Sections 2.3 and 2.4, the six sets of earthquake ground motions per Section 3.2, and the fragility functions of Section 3.3.

Huang's methodology uses Monte Carlo simulations and tens of thousands of realizations to compute a conditional probability of failure for each of the six intensities of earthquake shaking. For the risk calculations presented here, a simpler procedure involving Boolean algebra and probability theory is used instead of the tens of thousands of realizations. This procedure, which is described below, is sufficient to enable comparisons of risk for the conventionally founded and isolated GDNF at the INL and LANL sites.

In Figure 2-2, the Boolean notation $\cap$ denotes conjunction ($\wedge$ or AND) and $\cup$ denotes disjunction ($\vee$ or OR). In this fault tree, failure of a component/event immediately above an AND gate requires failure of all the components/events immediately below the gate. The failure of a component/event immediately an OR gate requires failure of one or more components/events immediately below the gate. The failure probability of the components/events in the fault tree can be calculated using the probability of failure each sub-component component (P_i, $i =$ the number of component). In the fault tree of Figure 2-2, and assuming independence of components 1 through 8, the probability of failure of the HVAC system is ($P_4 \times P_5$) and of the electrical component is ($P_1 + P_2 - P_1 \times P_2$).

The conditional probability of unacceptable performance $P_{UP}(S_{a,i})$ for shaking associated with spectral intensity $S_{a,i}$ can be calculated using the probability of failure (or unacceptable performance), $P_f(a)$, of each component. The fragility function for the component and demand on the component computed by nonlinear response-history analysis are used to calculate the probability of failure. (Consider the fragility function of Figure 3-4c. If the 2% damped spectral acceleration demand on the component (see Table 2-1) from response-history analysis is 2.8 g, the probability of failure is 0.5; if the demand is 6 g, the probability of failure is 0.94.) Demands on each component are computed for each response-history analysis, the probability of failure is computed for each component using its component-level fragility functios, and the fault tree of Figure 2-2 is then used, in conjunction with basic probability theory, to compute the probability of failure of the system conditioned on the input set of ground motion histories. This process is repeated for the other 29 sets of ground motions at the specific intensity, producing 30 values for the probability of failure at the intensity of earthquake shaking. The conditional

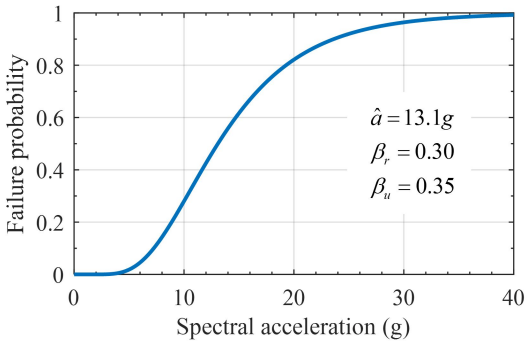

a. DC motor control center

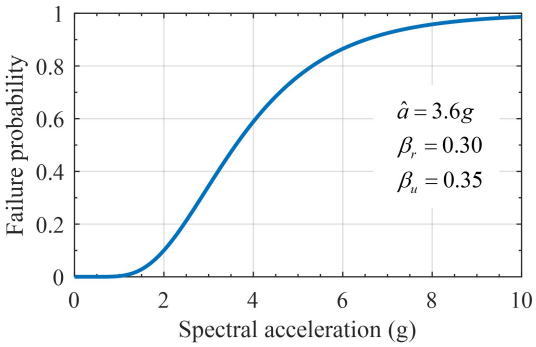

b. Battery

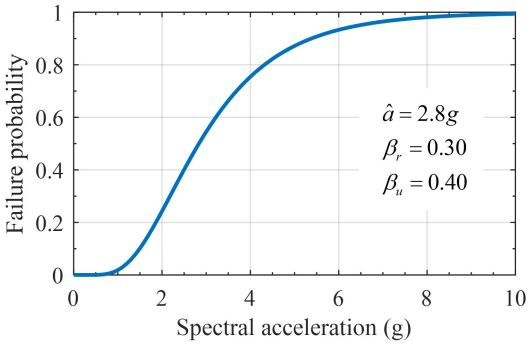

c. Reactor coolant pump

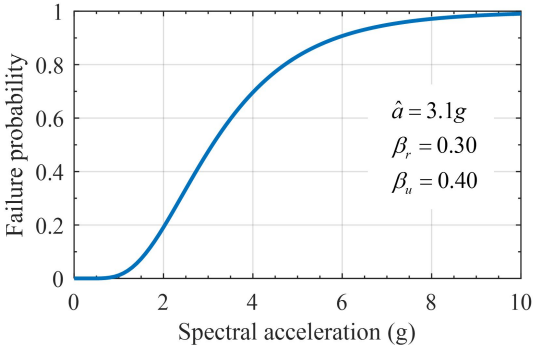

d. Air handler

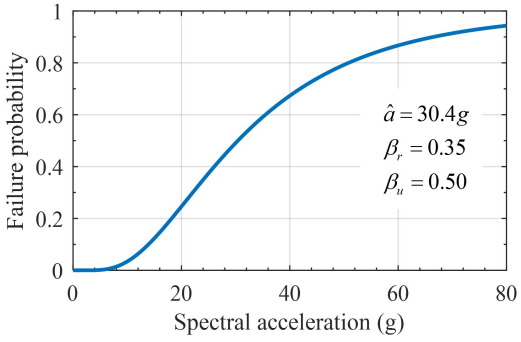

e. HVAC duct

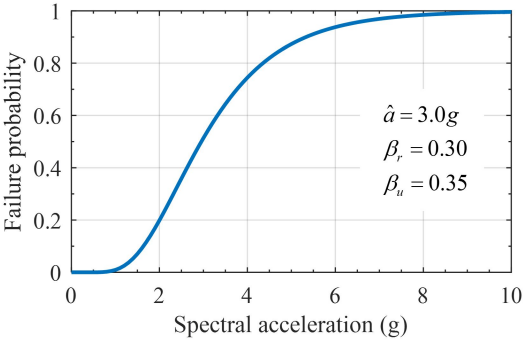

f. Containment

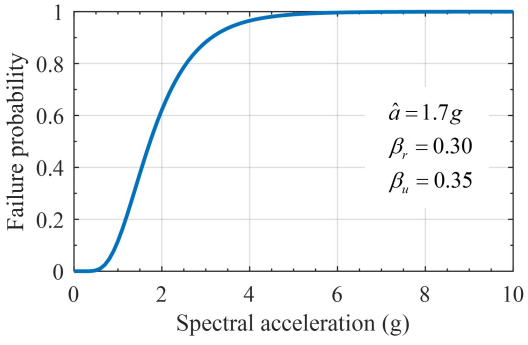

g. reactor pressure vessel

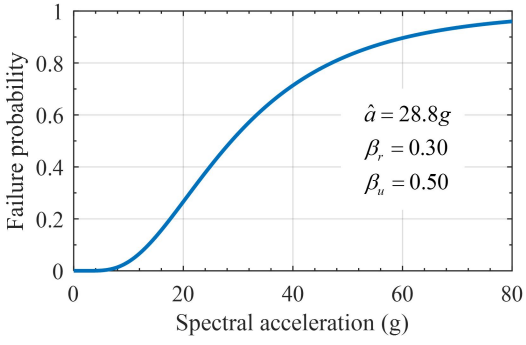

h. piping

Figure 3-4: Fragility curves for components at the INL site

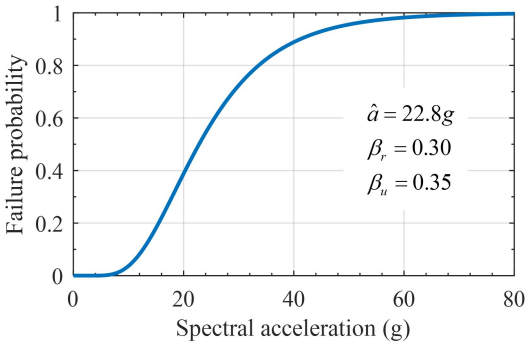

a. DC motor control center

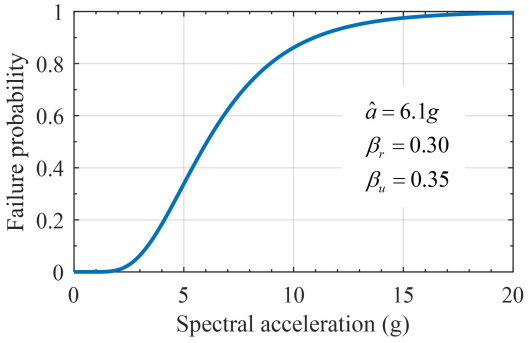

b. Battery

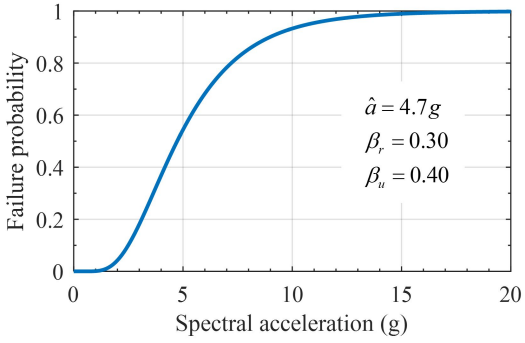

c. Reactor coolant pump

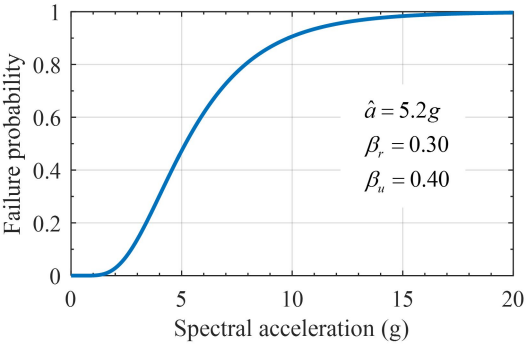

d. Air handler

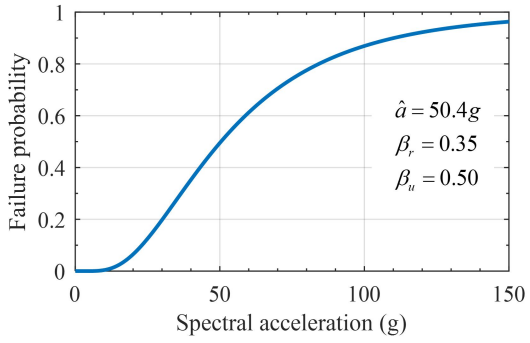

e. HVAC duct

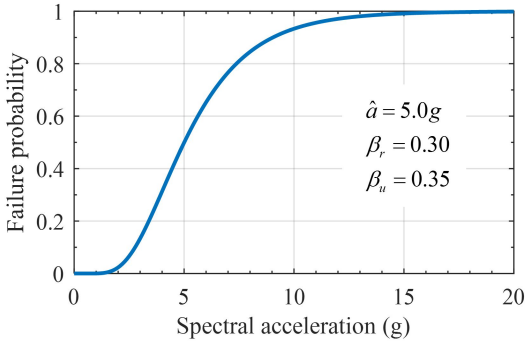

f. Containment

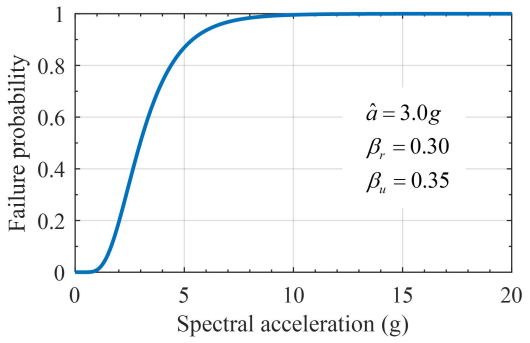

g. reactor pressure vessel

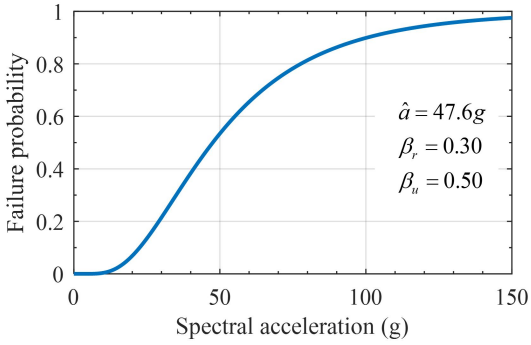

h. piping

Figure 3-5: Fragility curves for components at the LANL site

probability of failure, $P_{UP}(S_{a,i})$, at the intensity of shaking is the average of the 30 values. These values of $P_{UP}(S_{a,i})$ are multiplied by the corresponding mean annual frequency of the intensity of shaking, and then summed to compute the mean annual frequency of unacceptable performance.

Results of the risk calculations for the SSCs in the GDNF facility are presented in Table 3-4. In this table, $P_{UP}(S_{a,i})$ is the conditional probability of unacceptable performance for shaking associated with midpoint spectral intensity $S_{a,i}$, and other terms have been defined previously. Columns 3 and 5 of Table 3-1 map to columns 2 and 5 of Table 3-4. The fragility functions used for the risk calculations at the two sites are those derived in Section 3.3 for the conventionally founded construction: the functions are not recomputed here for each site based on the (smaller) demands associated with the response of the isolated construction.

The isolation of the GDNF facility, equipped with the components of Section 2.1.2, at the INL and LANL sites, reduces the seismic risk associated with horizontal earthquake shaking by approximately seven to eight orders of magnitude if the opportunity to reduce required seismic capacity, enabled by seismic isolation, is not taken. These significant reductions in risk confirm the observations of Huang et al. (2008b), who utilized simpler event and fault trees than those considered here and the same HCLPF-based approach to generate fragility functions. It is evident from the risk numbers presented here that there is considerable opportunity to reduce the seismic ruggedness (and thus cost) of the structures, systems and components installed in the isolated GDNF and still achieve levels of risk lower than those associated with the conventionally founded GDNF.

For the components considered here, including the locations of their points of attachment to the building and their fragility functions, and the hypothetical fault tree and event tree, the conditional probabilities of failure (i.e., loss of MAR) at DBE shaking (intensity i =2) for the conventionally founded structures at INL and LANL are higher than would be acceptable. As expected given how the fragility functions were derived, much of the total risk accrues for DBE and 1.5DBE shaking for both sites. Refinement of the calculation process and the estimate total risk could involve analysis at additional intensities of ground shaking at 0.75DBE, 1.25DBE and 1.75DBE.

3.5 Risk calculations for the isolation system

The risk calculations presented above focus on the SSCs contained within the GDNF structure. Not considered to date, and not part of the risk calculation process for conventionally founded structures, is the accident sequence associated with the failure of the isolation system.

Kumar et al. (2015, 2016) present a risk calculation procedure that focuses on the response of the seismic isolation system, and the results of those calculations are used here. Kumar performed risk calculations at sites of eight nuclear facilities in the United States, including the Idaho National Laboratory and Los Alamos National Laboratory. Calculations were performed using one definition of the DBE (a uniform hazard response spectrum with a return period of 10,000 years) and two definitions of beyond design basis earthquake (BDBE) shaking: 1) 150% DBE per Chapter 12 of ASCE 4-16, and 2) a uniform hazard response spectrum with a return period of 100,000 years per the draft seismic isolation NUREG/CR (Kammerer et al., forthcoming). Both results are presented below for both sites.

Table 3-4: Risk calculations for SSCs

a. INL

i	Conventionally founded GDNF			Isolated GDNF		
	$\Delta\lambda_i$	$P_{UP}(S_{a,i})$	$\Delta\lambda_i \times P_{UP}(S_{a,i})$	$\Delta\lambda_i$	$P_{UP}(S_{a,i})$	$\Delta\lambda_i \times P_{UP}(S_{a,i})$
1	2.16E-03	0.011	2.39E-05	3.19E-03	6.40E-16	2.04E-18
2	1.54E-04	0.240	3.69E-05	1.68E-04	1.51E-12	2.54E-16
3	3.53E-05	0.636	2.24E-05	3.55E-05	1.53E-10	5.42E-15
4	1.19E-05	0.878	1.05E-05	1.12E-05	3.79E-09	4.26E-14
5	4.78E-06	0.968	4.62E-06	4.28E-06	4.81E-08	2.06E-13
6	2.32E-06	0.993	2.31E-06	1.69E-06	3.35E-07	5.65E-13
$\lambda_{UP} = \sum_{i=1}^{6} P_{UP}(S_{a,i}) \cdot \Delta\lambda_{H,i}$			1.01E-04			8.19E-13

b. LANL

i	Conventionally founded GDNF			Isolated GDNF		
	$\Delta\lambda_i$	$P_{UP}(S_{a,i})$	$\Delta\lambda_i \times P_{UP}(S_{a,i})$	$\Delta\lambda_i$	$P_{UP}(S_{a,i})$	$\Delta\lambda_i \times P_{UP}(S_{a,i})$
1	7.94E-04	0.007	5.18E-06	6.97E-04	4.43E-14	3.09E-17
2	1.04E-04	0.203	2.11E-05	9.20E-05	1.61E-11	1.48E-15
3	3.50E-05	0.605	2.12E-05	3.33E-05	1.09E-09	3.64E-14
4	1.47E-05	0.861	1.26E-05	1.55E-05	1.82E-08	2.82E-13
5	7.21E-06	0.959	6.92E-06	8.28E-06	2.25E-07	1.86E-12
6	3.81E-06	0.989	3.82E-06	4.37E-06	1.36E-06	5.92E-12
$\lambda_{UP} = \sum_{i=1}^{6} P_{UP}(S_{a,i}) \cdot \Delta\lambda_{H,i}$			7.09E-05			8.10E-12

Chapter 12 of ASCE 4-16 and the draft seismic isolation NUREG/CR require that a) all production isolators be tested for DBE demands, as calculated by analysis, and b) prototype isolators be tested to a lateral displacement corresponding to 90th percentile BDBE shaking (or the clearance to the stop, if that is greater), with coexisting maximum (compression) and minimum (perhaps tension) axial forces. For prototype testing, the vendor must demonstrate 90% or greater confidence that the isolators can sustain these extreme demands. Both documents require the provision of a stop (or displacement restraint) at a displacement of no less than the 90th percentile BDBE displacement.

Figure 3-6 presents fragility functions for isolators tested to 95% confidence at the 90th percentile displacement, where the BDBE is characterized per the draft isolation NUREG. Similar fragility functions are anticipated for the isolators of Section 2.4 because large margins are present on the displacement and axial force capacities of the chosen LR isolator at 150% DBE shaking.

Figure 3-6a presents the functions for the case where no stop is present. Figure 3-6b presents the corresponding functions if the stop is installed at the 90th percentile BDBE displacement. In the legend below the figures, the curves for the Idaho Falls and Los Alamos are identified. In this figure, the vertical axis is the probability of failure of an individual isolator and the horizontal axis is multiples *m* of DBE shaking.

The Kumar et al. calculations make two important assumptions: 1) isolator capacities are fully correlated, and 2) isolator demands are fully correlated. By making these assumptions, the fragility function for the isolation system can be taken as that for an individual isolator. The first assumption is reasonable if the isolation system is composed of only one type of bearing because both ASCE 4-16 and the draft isolation NUREG/CR demand very high quality control on the production of isolators.

The second assumption was necessary to develop a calculation process and sample values of risk but is very conservative for isolation systems composed of 10s of bearings and extremely conservative for isolation systems composed of 100s of isolators. Prototype tests of a given type and size of bearing will use the maximum lateral displacement (see above) of the isolator in beyond design basis shaking and the corresponding maximum and minimum axial forces. Although the isolators in a system may experience similar lateral displacements for a given three-component set of earthquake ground motions (if torsion is negligible), all bar one will experience axial demands smaller than the maximum and minimum values used for prototype testing and performance evaluation. Reducing the maximum compressive and minimum tensile axial loads on an isolator will increase its lateral displacement capacity, effectively shifting its fragility functions to the right (as drawn in Figure 3-6).

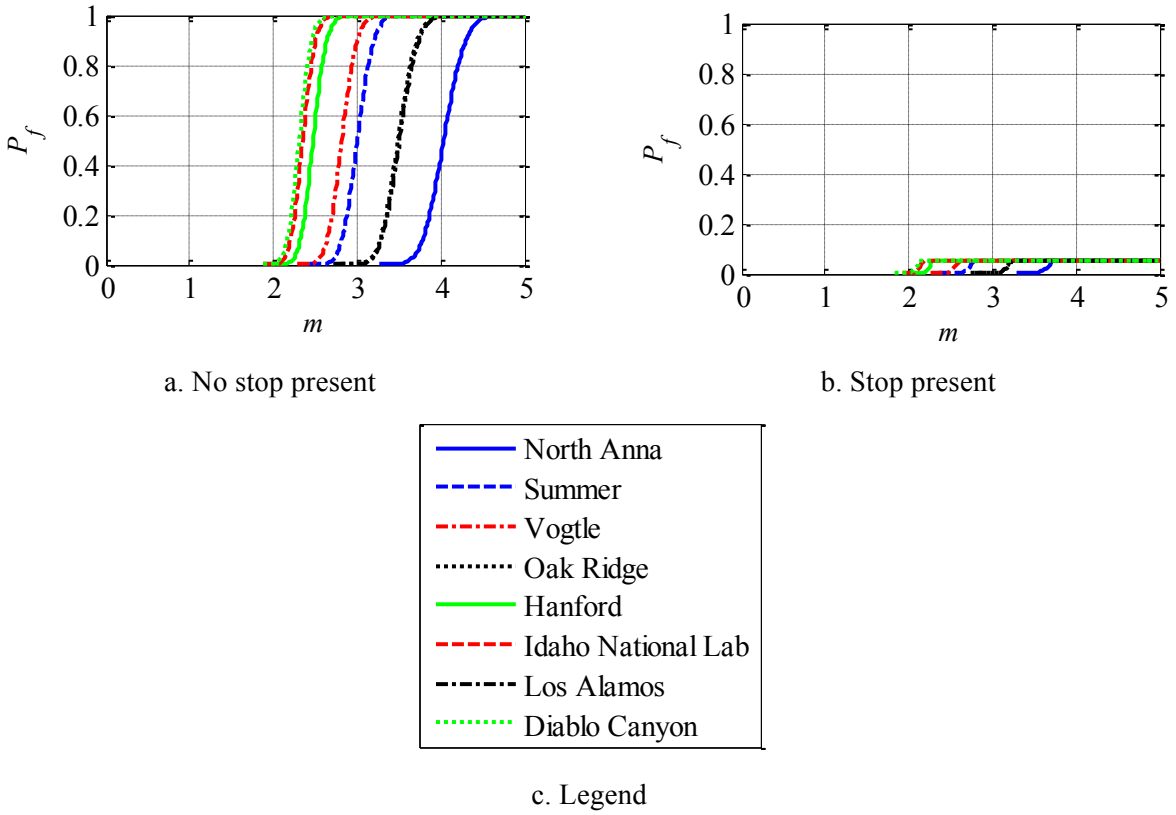

a. No stop present

b. Stop present

c. Legend

Figure 3-6: Fragility functions for isolators prototype tested to the recommendations of the draft seismic isolation NUREG/CR with 95% confidence (from Kumar et al. 2016)

The isolation system proposed in Section 2 for the GDNF is composed of 38 isolators. Both Chapter 12 of ASCE 4-16 and the draft seismic isolation NUREG/CR require the design of the basemat (above the isolation plane, see Figure 1-1) to span across isolators that have been assumed to fail in the short term to support gravity loads. The failure of one isolator is not allowed to trigger the failure of the isolation system. Indeed, the presence of stiff, strong walls in the GDNF superstructure would permit the failure (short-term loss of axial load capacity) of a number of isolators in the system of 38. (In an isolated nuclear power plant, which might be supported by 500 isolators, 10s of isolators would have to fail for the isolation system to be rendered ineffective.)

The mean annual frequency of unacceptable performance of the isolation system is calculated by Kumar et al. (2015, 2016) to be 4×10^{-7} at both INL and LANL if the recommendations of the isolation NUREG/CR are followed, including the provision of a stop, and prototype isolators are tested to achieve 95% confidence. If the recommendations of Chapter 12 of ASCE 4-16 are followed, including the provision of a stop, and prototype isolators are tested to achieve 95% confidence, the mean annual frequency of unacceptable performance of the isolation systems at INL and LANL are 1×10^{-6} and 2.1×10^{-6}, respectively. These risk numbers do not consider either a) the weak correlation of peak demands (horizontal displacement and maximum/minimum axial force), or b) the redundancy imposed by the mandatory language of ASCE 4-16 and the recommendations of the draft isolation NUREG. Importantly, failure of the isolation system is assumed to trigger unacceptable performance (e.g., loss of containment) and that is unlikely because the GDNF cannot move a) horizontally beyond the stop, and b) vertically more than a few inches because the damaged isolators will still be in place. As such, these mean annual frequencies of unacceptable performance are very conservative (too high).

3.6 Managing risk using seismic isolation

The risk associated with the failure of the seismic isolation system will likely range between 10^{-7} and 10^{-8} once the weak correlation of demands on individual isolators and the positive effect of redundancy are characterized, depending on which set of rules (ASCE 4-16 or the draft seismic isolation NUREG/CR) are followed. These mean annual frequencies of unacceptable performance are extremely small but they are four to five orders of magnitude greater than those of the SSCs in the isolated GDNF per Table 3-4. The seismic risk portfolio in the isolated facility is unbalanced: all of the risk is associated with the isolation system. An increase in the mean annual frequency of unacceptable performance in the SSCs from between 10^{-11} and 10^{-12} (see Table 3-4) to between 10^{-8} and 10^{-9} would not increase the total seismic risk in a meaningful way (and it is still very low) but may enable a very significant reduction in the required ruggedness of the SSCs in an isolated facility. A significant reduction in the required seismic ruggedness (but still meeting target performance goals by a wide margin) will reduce the cost of the SSCs, with the percentage reduction in cost being component specific. Huang et al. (2008b) provides some sample calculations on the possible reductions in required seismic strength (see Figure 5.37 of that reference).

4. COST IMPLICATIONS OF ISOLATING NUCLEAR STRUCTURES

4.1 Introduction

The cost of constructing safety-related nuclear structures is driven in significant part by considerations of the effects of earthquake shaking, especially in nuclear power plants. Capital cost can be reduced by the use of advanced numerical tools such as those for nonlinear site-response (e.g., Bolisetti et al., 2014), soil-structure interaction analysis (e.g., Coleman et al. 2015), and advanced probabilistic risk assessment (e.g., Huang et al. 2008b, 2011a, 2011b; Bolisetti et al. 2015; Coleman et al. 2016). Another strategy to decrease capital costs is the reduction in seismic demands, which can be accomplished using seismic isolation and/or supplemental damping systems.

Despite the broad agreement in the nuclear community that consideration of earthquake effects adds substantially to the cost of nuclear structures, only one study has been performed on the subject to the knowledge of the authors. This study was first published as a NUREG report (Stevenson 1981) and later updated (Stevenson 2003). The cost estimates provided here draw heavily on the Stevenson studies because they provide the only known source of data that relates increases in plant cost with corresponding increases in seismic hazard. Although Stevenson performed his studies on nuclear power plants, the general results and trends are assumed to be a) still current, and b) applicable to a broad range of safety-related nuclear structures, such as those discussed here.

Stevenson (1981) calculated the incremental cost for increasing the seismic capacity of a sample 1100 to 1300 MW nuclear power plant, from zero to a safe shutdown earthquake (SSE) peak ground acceleration (PGA) of between 0.2g and 0.6g. His study included only direct costs such as those associated with strengthening of structure, foundations and supports, qualification of equipment and additional engineering services. Other costs such as additional licensing review, additional construction time and cost of money, and non-A/E engineering were not considered. The incremental seismic costs were calculated separately for each of the following categories:

1. *Site preparation and foundation cost*: Stevenson (1981) estimated only the incremental foundation cost when the facility was constructed on liquefiable soils. No estimates are made of the cost increase for other sites and soil conditions. (Greater seismic demands would require thicker basemats, more reinforcement, additional excavation, etc.)
2. *Cost of building structures*: The increased cost of building structures addressed the greater volume of concrete and reinforcement required to resist higher seismic forces. Stevenson (1978) suggested that this cost increased linearly with SSE PGA from 0.2g to 0.6g.
3. *Cost of mechanical components and electrical components*: Mechanical components include vessels, tanks, heat exchangers, pumps, valves, and fans. The increase in seismic cost in this category is due to the required strengthening of the anchorages and supports for these components. Another source of increase in cost is the seismic qualification of equipment for demands greater than those for which the component was previously certified, which entails extensive laboratory testing and engineering time. Stevenson proposed an increase in cost that increased linearly with the SSE PGA, beyond a nominal value of 0.15g. Stevenson (1981) also polled equipment vendors to gain a sense for the cost of qualifications as a function of shaking intensity. Although the survey results were highly variable, it was clear that the cost of equipment qualification for high seismic demands was greater than that for low seismic demands.

4. *Electrical components*: Electrical components include generators, control cabinets, switch gear, and motors. Similar to mechanical components, the increase in cost in this category is due to stiffening and strengthening of supports. The cost of qualification of electrical components also increases with SSE PGA. Identical to mechanical components, Stevenson (1981) assumed that the cost increase in this category is directly proportional to SSE PGA, beyond a nominal value at 0.15g.
5. *Mechanical and electrical distribution systems*: Distribution systems include piping, tubing, ventilation ducts, electrical conduits, and raceways. This category is the source of the most significant increase in cost due to seismic requirements. The additional costs arise from the strengthening of these systems through additional supports, and snubbers in case of piping systems. Stevenson (1981) proposed that the additional cost due to strengthening of the distribution systems was proportional to the square root of the SSE PGA, beyond a nominal PGA of 0.10g.

Engineering cost: Engineering cost includes the architect and engineer (A/E) fees and the cost of computing time. Stevenson (1981) proposed that the engineering cost increased linearly with SSE PGA.

Table 4-1 summarizes the breakdown of the cost increments estimated by Stevenson in 1981 for a 1200 MW (approximately) light water reactor, which had a total overnight capital cost of $1,053 million (1977 dollars). For example, 23% of the total cost increment associated with an increase in the design PGA from 0 g (no seismic consideration) to 0.2 g is associated with auxiliary components. The table shows that the major sources of cost increase are engineering, distribution systems and auxiliary and nuclear steam supply system components (NSSS). The auxiliary and NSSS components compose the mechanical and electrical components described above. The cells for foundations have no entries because Stevenson did not report cost increases at either PGA for foundations on non-liquefiable soil, and the sites considered for cost estimation in this study are not susceptible to liquefaction.

Stevenson (1981) also estimated the total cost incurred due to seismic design (or seismic considerations) as a percentage of the total overnight capital cost of the power plant. Figure 4-1a presents the cost increase for seismic design, as a percentage of the total plant cost, as a function of the SSE PGA. The cost increase for seismic design ranges from about 2% at a PGA of 0.1g to about 9% at a PGA of 0.65g. A similar estimate from a later study by Stevenson (2003) is presented in Figure 4-1b. Larger increases are seen here: 9% at a PGA of 0.2g to about 18% at 0.6g. The reason for the increase is not given.

The study presented in the following section uses the results of Stevenson studies to calculate the costs of seismic design for the three cases listed in Section 1.2. Although this study deals with DOE structures and not nuclear power plants, the Stevenson data are the most applicable known available.

Table 4-1: Percentage breakdown of total seismic design cost increases for a large light-water reactor founded on non-liquefiable soil as a function of design PGA (adapted from Stevenson 1981)

	% increase at design PGA	
Category	**= 0.2 g**	**= 0.6 g**
Foundations[1]	--	--
Structures	5	8
Auxiliary components	23	18
Nuclear steam supply system components (NSSS)	6	18
Distribution systems	10	20
Engineering	43	26
Turbine	1	1
Site studies including seismology	12	9
Total	100	100

1. Cost increases not reported for foundations

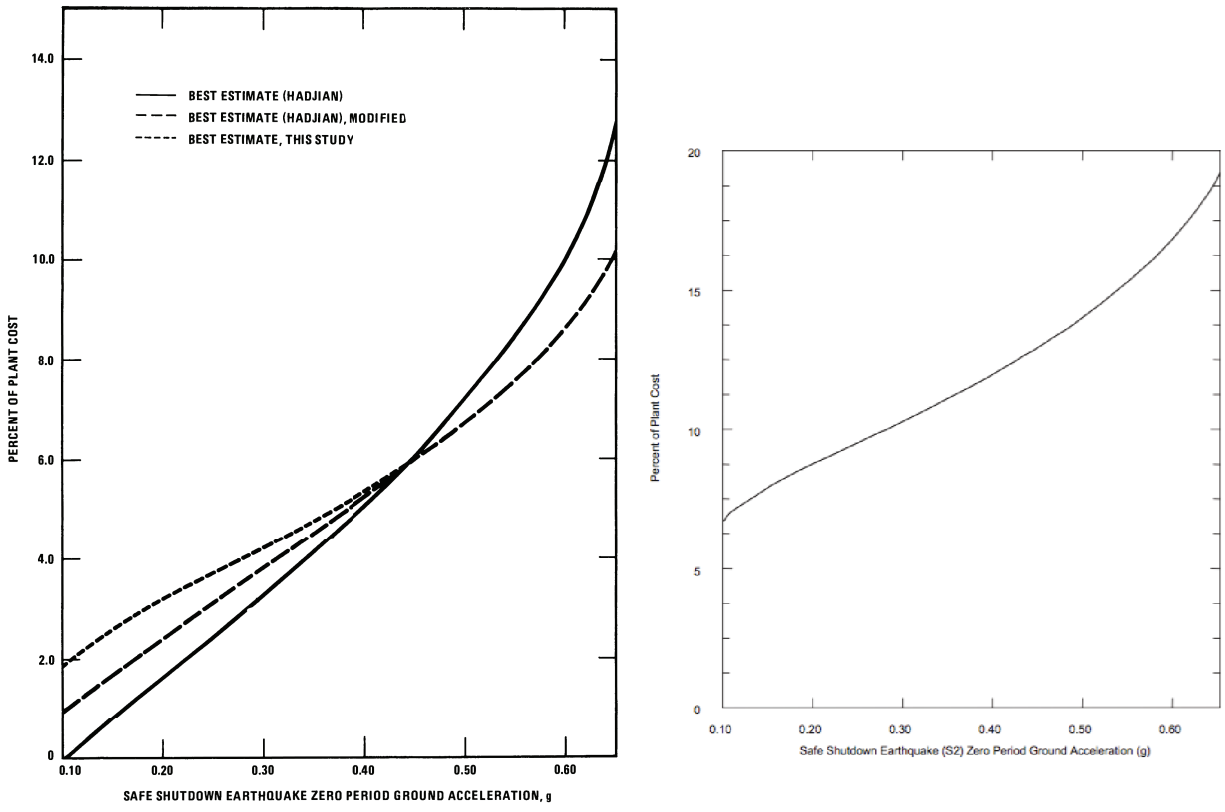

a. Stevenson (1981) b. Stevenson (2003)

Figure 4-1: Cost of seismic design as a percentage of total plant cost as a function of SSE PGA

4.2 Cost estimates

4.2.1 Calculation of overnight capital costs

The overnight capital cost (OCC) is the total cost of a facility excluding indirect costs such as cost escalation and interest during the construction period. The OCC for GDNF is estimated to be around $550 million in 2016 dollars. For the purpose of estimating costs in this study, the total cost of the facility is divided into six categories: (1) foundation, (2) structures, (3) mechanical and electrical systems, (4) distribution systems, (5) engineering, and (6) other miscellaneous costs. This categorization not only enables the use of the results of the Stevenson studies but also keeps this report generic. Representative costs are estimated based on the breakdown of the OCC described in Stevenson (2003) and presented in Table 4-2. The costs presented in this table are for a large light-water reactor and are based in Year 2000 dollars. Note that Stevenson (2003) provides a more detailed breakdown of the OCC than that presented here, but the data is converted into above categories to enable calculations. These costs are comparable to other OCC estimates for nuclear power plants (EIA, 2013; EPRI, 2009).

Table 4-2: Overnight capital costs for a large light-water reactor and the GDNF (adapted from Stevenson 2003)

	Cost in USD, millions	
Category	**LWR, 2000 dollars**	**GDNF, 2016 dollars**
Foundation[1]	16	5
Structure	162	53
Mechanical and electrical systems	773	251
Distribution systems	188	61
Engineering	356	116
Other	198	64
Total	**1693**	**550**

1. Assumed to be 10% of structure cost

The OCCs for the components of the GDNF, with an estimated total cost of $550 million USD, are estimated by scaling down the total cost of the OCCs of the large light-water reactor by category. The corresponding OCCs for the GDNF are presented in the third column of Table 4-2, in 2016 dollars. This OCC is *assumed* to be the cost of the structure with minimum seismic design costs.

4.2.2 Calculation of seismic design costs

The cost impact of implementing seismic isolation is calculated by comparing the total cost (OCC + seismic design cost) for the three cases of Section 1.2. The seismic cost for each of the component categories listed in Table 4-2 is first calculated as a function of the design PGA. (Note that PGA is not necessarily a good descriptor of seismic demand and thus cost, but it is used here in lieu of an alternate.) Seismic design cost functions are created by calculating the seismic costs at two PGA values (0.2 g and 0.6 g), and interpolating between them, based on the category-specific variation in seismic cost with PGA, as described in Section 4.1. For example, the seismic design cost of *structure* is first calculated at

the PGA= 0.2 g and PGA = 0.6 g, and the function for this category is calculated assuming that the cost increases linearly with PGA.

The total seismic design costs of the GDNF at PGA= 0.2 g and PGA= 0.6 g are assumed to be 11% and 20%, respectively, based on the curve in Figure 4-1b. The individual seismic design costs of the components are calculated using the breakdown of the seismic design costs presented in Table 4-1. The so-calculated seismic design costs for the GDNF are presented in Table 4-3. The cost curves calculated for each category are presented in Figure 4-2.

For the isolated GDNF facility at LANL (Case 3 in Section 1.2), it is assumed that the seismic design of structures and components is governed by the peak acceleration of the basemat above the isolation system, as opposed to PGA. For the GDNF, the peak acceleration of the basemat is less than 0.1 g for the design range of PGA of 0.2 g to 0.6 g considered in this study. Therefore, it is assumed that the seismic design cost does not increase beyond the value for the conventionally founded facility for a PGA = 0.15 g.

The cost of implementing seismic isolation is estimated using information at hand for the isolation of an advanced reactor. Implementing isolation requires three additional construction tasks: 1) design, procurement and installation of the isolators (less than $0.75M USD for the GDNF considered here), 2) over excavation to accommodate the additional foundation and pedestals (see Figure 1-1), and 3) construction of the reinforced concrete foundation, moat walls and pedestals. Given the generic nature of the sample facility, the cost of isolation in Case 3 is assumed to be twice the cost of the foundation in the conventionally founded GDNF.

Table 4-3: Seismic design costs for GDNF at 0.2g and 0.6g PGA in 2016 dollars (millions)

Category	**0.2g PGA**	**0.6g PGA**
Foundation	< 1	2
Structures	2	6
Mechanical and electrical systems	9	24
Distribution systems	36	53
Engineering	14	23
Other	1	4
Total	**62**	**112**
Percentage of OCC	**11**	**20**

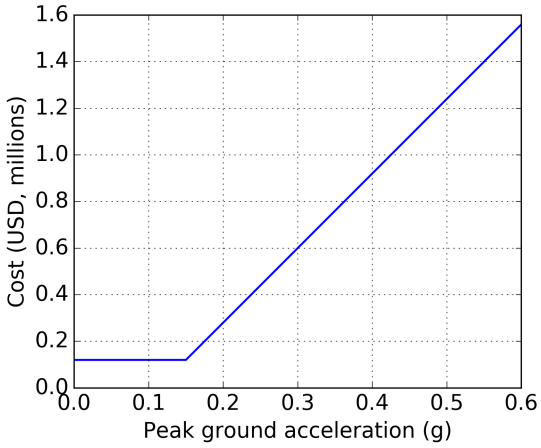

a. foundation

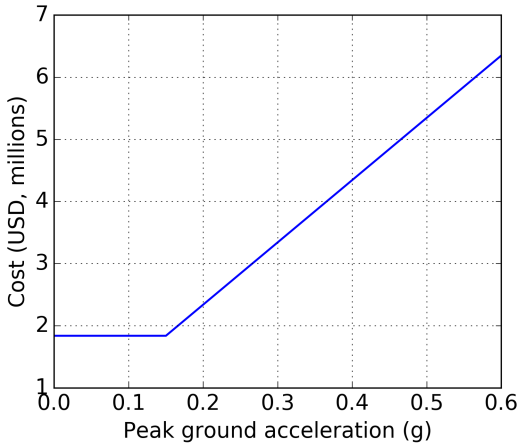

b. structure

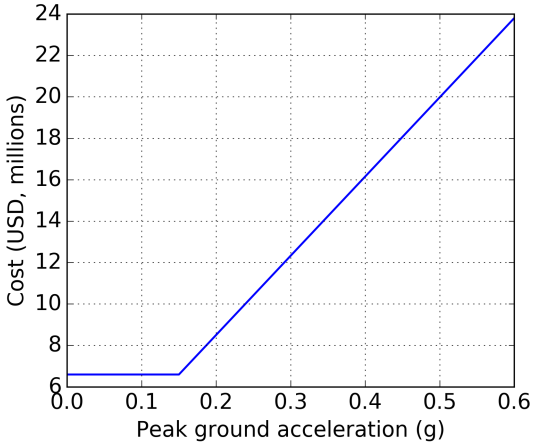

c. mechanical and electrical systems

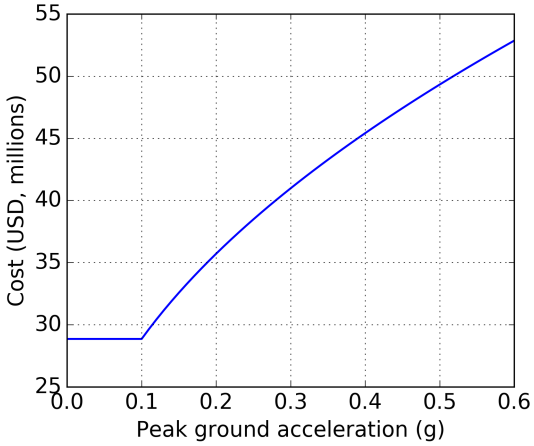

d. distribution systems

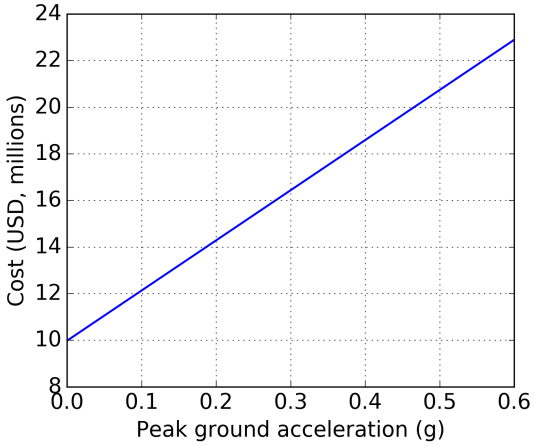

e. engineering

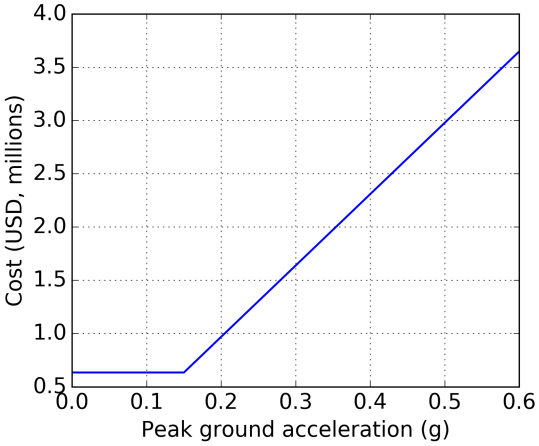

f. other

Figure 4-2: Seismic design cost versus peak ground acceleration by category

4.2.3 Cost calculations

The total seismic design cost for each case and PGA is the sum of the corresponding seismic design costs of the component categories. The design-basis earthquake at INL is 0.3 g and at LANL is 0.5 g. Figure 4-3 presents total cost as a function of PGA for the conventional and base isolated structures. At small values of PGA, the cost of the isolated structure is higher than that of the conventional structure, which is obvious. At a PGA of 0 g, there is no seismic cost for the conventionally founded GDNF and the difference in cost (conventional versus isolated) is the cost of tasks 1, 2 and 3 identified in the previous section. The conventional-to-isolated threshold for this example is PGA= 0.23 g, beyond which the total cost of the isolated facility is less than that of its conventional counterpart. There is a clear benefit of isolation (to the sample GDNF) at a PGA= 0.3 g (the INL site) and a very significant benefit at a PGA = 0.6 g (the LANL site).

Table 4-4 presents the seismic cost, total cost and the seismic cost as a percentage of the total cost for the three cases of Section 1.2. Isolation is beneficial in terms of reduced capital cost at both the INL and LANL sites, with the greatest benefit at the site with the higher design-basis PGA, namely, LANL.

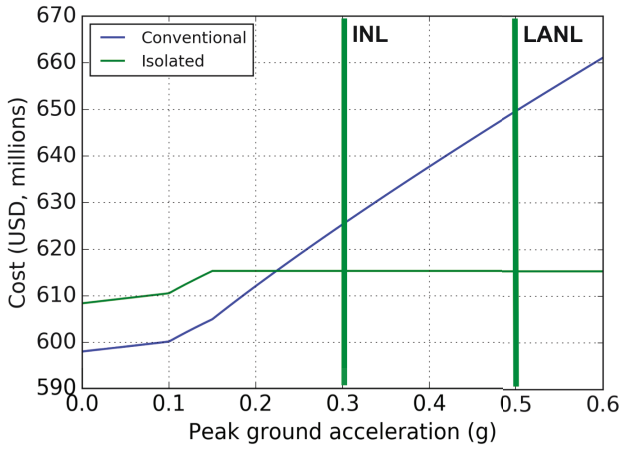

Figure 4-3: Total cost as a function of PGA for conventional and isolated variants of the GDNF at INL and LANL

Table 4-4: Cost estimates for GDNF construction at INL and LANL

Case	Seismic cost (millions)	Total cost (millions)	Percentage of total cost
1: INL, conventional construction	72	627	13
2: LANL, conventional construction	100	655	18
3: LANL, isolated construction	65	620	11

5. SUMMARY, CONCLUSIONS AND FUTURE WORK

5.1 Summary and conclusions

This report provides a framework for assessing the benefits of seismic isolation and exercises the framework on a Generic Department of Energy Nuclear Facility (GDNF). These benefits are (1) reduction in the risk of unacceptable seismic performance and a dramatic reduction in the probability of unacceptable performance at beyond-design basis shaking, and (2) a reduction in capital cost at sites with moderate to high seismic hazard. The framework includes probabilistic risk assessment and estimates of overnight capital cost for the GDNF.

The risk assessments and cost estimates are performed for the GDNF for three cases:

1. GDNF is located at a site of low to moderate seismic hazard and constructed on a conventional (non-isolated) foundation
2. GDNF is located at a site of high seismic hazard and constructed on a conventional foundation
3. GDNF is located at the same site of high seismic hazard as Case 2, but seismically isolated

In this study, the DOE site at Idaho National Laboratory (INL) is chosen for the site of low to moderate seismic hazard (Case 1). The Los Alamos National Laboratory (LANL) is chosen for to represent the site of high seismic hazard site (Cases 2 and 3).

Seismic probabilistic risk assessment (SPRA) is performed using the methodology proposed by Huang et al. (2008), and the risk assessment for the isolators is performed using the methodology described in Kumar et al. (2015, 2016). The Kumar methodology for generating fragility functions for isolators can be integrated into the Huang SPRA methodology but wasn't for this study. A time-based risk assessment is performed for all three cases by assuming a generic safety system and associated components.

The costs estimates use results and data from Stevenson (1981, 2003), who calculated the seismic design costs of a large light-water reactor at design peak (horizontal) ground accelerations (PGAs) of 0.2 g and 0.6 g for various categories of structures, systems and components (SSCs) in the power plant. The seismic costs of each component category are scaled down to the total overnight capital cost (OCC) of the GDNF and interpolated between PGAs of 0.2 g and 0.6 g to calculate the seismic design cost of the GDNF at the INL and LANL sites. The cost of the construction required to implement the seismic isolation system (over excavation, additional basemat, walls and pedestals, and fabrication, testing and supply of the isolators) was taken was twice the cost of the foundation of the conventionally constructed (non isolated) GDNF.

The following conclusions are drawn from the study:

1. The implementation of seismic isolation in the GDNF results in seismic risks that are several orders of magnitude smaller than those of the conventionally founded facility for the same seismic hazard and SSC capacities. The reduction is possible due to drastically smaller horizontal seismic demands, which also result in very low probabilities of unacceptable performance at levels of shaking even significantly greater than design basis.
2. The implementation of seismic isolation in the GDNF reduces the total construction cost for design peak horizontal acceleration greater than approximately 0.2 g. The percentage reduction in cost

associated with the use of isolation increases beyond this threshold value and could be very significant for sites with moderate to high seismic hazard.

3. The framework described in this study can be used to assess the benefits of seismic isolation of any safety-related facility. The use of the framework will result in better estimates of seismic risk and a better understanding of the financial costs and benefits if seismic isolation is proposed for use at new DOE facilities.

The studies reported herein were hampered by a lack of modern data on the effect of seismic forces on the design, fabrication and qualification of structures, systems and components (SSCs) in safety-related nuclear structures. The shaking-intensity threshold beyond which the use of isolation leads to reductions in construction cost were based on the studies of Stevenson (1982, 2003), neither of which may be directly applicable to a broad range of safety-related nuclear structures, and may no longer be appropriate for new build NPPs. Fragility data for modern SSCs are not widely available. The lack of fragility data that address the effects of vertical earthquake shaking required the study to set it aside as a seismic input to both the conventionally founded and isolated GDNF.

Not characterized in this report are two benefits of seismic isolation: 1) the ability to manage significant increases in seismic hazard at a site in the years and decades after construction, and 2) the opportunity to move NPP designs that have been certified for sites of low-to-moderate seismic hazard to sites of higher seismic hazard. In the first case, an increase in seismic hazard in a conventionally founded facility will translate into an increase in seismic risk unless SSCs are hardened. In an isolated facility, new isolators, with different mechanical properties could be used to replace the original isolators, with no need for new construction (and new SSCs), and no downtime associated with the upgrades.

5.2 Future work

The study presented in this report calculates the cost and risk benefits independently. The seismic risk calculated for the isolated structure in Case 3 results in risks that are several orders of magnitude lower than the performance goals of ASCE 43. This reduction in risk can be leveraged to reduce the capacities of the components until the final risk is closer to the performance goal. The reduction in capacities will lead to a reduction in cost. Although Huang et al. (2008b) characterized the possible reduction in seismic capacity of SSCs in NPPs enabled by the use of base isolation, work is needed to a) integrate this activity into the risk-based design framework described herein, and b) address other types of nuclear safety-related structures.

Work is needed to study the effects of correlations on demands and capacities of isolators. To date, isolator capacity is assumed to represent isolation-system capacity, which may be reasonable for a system of a few isolators but is unreasonable (and very conservative) for a system composed of 10s or 100s of isolators. Isolator capacities should be highly correlated because strict quality control procedures must be followed for bearing fabrication. Demands on isolators are assumed at this time to be fully correlated but this is extremely unlikely. Not all isolators will experience demands at the same instant in time equal to the maximum lateral displacement and axial force demand used in prototype testing to establish the fragility of the critically loaded isolator.

Redundancy in the isolation system, afforded by a stiff and strong basemat above the plane of isolation capacity in a nuclear facility, also needs to be quantified to enable more robust estimates of risk.

The cost estimate performed in this study is specific to the OCCs assumed for the GDNF. However, DOE structures are diverse and cost characteristics and contents vary by size and function. New cost data are needed for families of components and systems used in safety-related nuclear structures and NPPs, where cost is linked directly to how the component is supported and the level of excitation (or seismic hazard) at the points of attachment. Such data are needed for project-specific implementation of the framework introduced in this report.

Fragility functions for specific components were back calculated using a HCLPF-based strategy implemented in Huang et al. (2008b). Vulnerability of SSCs to the effects of vertical shaking was not considered. Future work on the topics described in this report would benefit from the use of component-specific fragility functions (e.g., real components subjected to earthquake simulator testing) that a) would address the effects of vertical shaking, and b) characterize the relative importance of vertical versus horizontal shaking.

5.3 Benefits of this study

The outcomes of this study are expected to benefit the nuclear industry by providing a framework to calculate the costs and benefits of seismic isolation. The framework was applied to an exemplar GDNF. The study showed that base isolation could be used to simultaneously increase safety and reduce construction cost. Fragility and construction cost data for modern SSCs would enable more accurate estimates of the benefits to be made.

The outcomes of the study reinforce the importance of infusing risk calculations into every step of the design process, enabling timely decision making to achieve with *high confidence* both *target levels of risk* at the *minimum possible construction cost*. Advanced technology such as seismic isolation and damping devices and advanced numerical simulation tools will play an important role in such decision-making.

This study has partially funded a Ph.D. student at the University at Buffalo and a research scientist at INL in FY2016. The information presented in this report will be condensed into a) an article to be published in a peer reviewed journal, and b) a paper to be presented at an upcoming meeting of IASMiRT.

6. REFERENCES

American Society of Civil Engineers (ASCE). (2005). "Seismic design criteria for structures, systems and components in nuclear facilities." ASCE/SEI Standard 43-05, Reston, VA.

American Society of Civil Engineers (ASCE). (2010). "Minimum design loads for buildings and other structures." ASCE/SEI Standard 7-10, Reston, VA.

American Society of Civil Engineers (ASCE). (2016). "Seismic analysis of safety-related nuclear structures and commentary." ASCE/SEI Standard 4-16, Reston, VA.

Bolisetti, C., Whittaker, A. S., Mason, H. B., Almufti, I., and Willford, M. (2014). "Equivalent linear and nonlinear site response analysis for design and risk assessment of safety-related nuclear structures." *Nuclear Engineering and Design*, 275, 107-121.

Bolisetti, C., Coleman, J. L., Talaat, M., and Hashimoto, P. (2015). "Advanced seismic fragility modeling using nonlinear soil-structure interaction analysis." INL/EXT-15-36375, Idaho National Laboratory, Idaho Falls, ID.

Bozorgnia, Y., and Campbell, K. W. (2004). "The vertical-to-horizontal response spectral ratio and tentative procedures for developing simplified V/H and vertical design spectra." *Journal of Earthquake Engineering*, 8(2), 175-207.

Coleman, J. L., Bolisetti, C., and Whittaker, A. S. (2015). "Time-domain soil-structure interaction analysis of nuclear facilities." *Nuclear Engineering and Design*, 298, 264-270.

Coleman, J. L., Bolisetti, C., Veeraraghavan, S., Parisi, C., Prescott, S. R., Gupta, A., and Kammerer, A. M. (2016). "Multi-hazard advanced seismic probabilistic risk assessment tools and applications." INL/EXT-16-40055, Idaho National Laboratory, Idaho Falls, ID.

Constantinou, M. C., Whittaker, A. S., Kalpakidis, Y., Fenz, D. M., and Warn, G. P. (2007). "Performance of seismic isolation hardware under service and seismic loading." MCEER-07-0012, University at Buffalo, The State University of New York, Buffalo, NY.

Energy Information Agency (EIA). (2013). "Updated capital cost estimates for utility scale electricity generating plants." Washington, D.C.

Electric Power Research Institute (EPRI). (2003). "Seismic probabilistic risk assessment implementation guide." 1002989, Electric Power Research Institute, Palo Alto, CA.

Electric Power Research Institute (EPRI). (2009). "Program on technology innovation: integrated generation technology options." 1019539, Palo Alto, CA.

Electric Power Research Institute (EPRI). (2013). "Seismic probabilistic risk assessment implementation guide." 3002000709, Palo Alto, CA.

Federal Emergency Management Agency (FEMA). (2012). "Seismic performance assessment of buildings, Volume 1." FEMA P-58-1, Washington, D.C.

Hadjian, A. H. (1981). "On the correlation of the components of strong ground motion - Part 2." *Bulletin of the Seismological Society of America*, 71(4), 1323-1331.

Hancock, J., Watson-Lamprey, J., Abrahamson, N. A., Bommer, J. J., Markatis, A., McCoy, E. and Mendis, R. (2006). "An improved method of matching response spectra of recorded earthquake ground motion using wavelets." *Journal of Earthquake Engineering*, 10: S1, 67-89.

Huang, Y.-N., Whittaker, A. S., and Luco, N. (2008a). "Maximum spectral demands in the near-fault region." *Earthquake Spectra*, 24(1), 319-341.

Huang, Y.-N., Whittaker, A. S., and Luco, N. (2008b). "Performance assessment of conventional and base-isolated nuclear power plants for earthquake and blast loadings." MCEER-08-0019, University at Buffalo, The State University of New York, Buffalo, NY.

Huang, Y.-N., Whittaker, A. S., and Luco, N. (2009a). "Orientation of maximum spectral demand in the near-fault region." *Earthquake Spectra*, 25(3), 707-717.

Huang, Y.-N., Whittaker, A. S., Kennedy, R. P. and Mayes, R. L. (2009b). "Assessment of base-isolated nuclear structures for design and beyond-design basis earthquake shaking." MCEER-09-0008, University at Buffalo, The State University of New York, Buffalo, NY.

Huang, Y.-N., Whittaker, A. S., and Luco, N. (2011a). "A seismic risk assessment procedure for nuclear power plants, (I) methodology." *Nuclear Engineering and Design*, 241, 3996-4003.

Huang, Y.-N., Whittaker, A. S., and Luco, N. (2011b). "A seismic risk assessment procedure for nuclear power plants, (II) application." *Nuclear Engineering and Design*, 241, 4004-4011.

Huang, Y.-N., Whittaker, A. S., and Luco, N. (2011c). "Establishing maximum spectral demand for performance-based earthquake engineering: collaborative research with the University at Buffalo and the USGS." *USGS Technical Report: Award Number 08HQGR0017*, United States Geological Survey, Reston, VA.

Huang, Y.-N., W.-Y. Yen, W.-Y., and Whittaker, A. S. (2016). "Correlation of horizontal and vertical components of strong ground motion for response-history analysis of safety-related nuclear structures." *Nuclear Engineering and Design*, http://dx.doi.org/10.1016/j.nucengdes.2016.09.036

Kammerer, A., Whittaker, A. S., and Coleman, J. L. (2015). "Regulatory gaps and challenges for licensing advanced reactors using seismic isolation." INL/EXT-15-36945, Idaho National Laboratory, Idaho Falls, Idaho.

Kammerer, A., Whittaker, A. S., and Constantinou, M. C. (forthcoming). "Technical considerations for seismic isolation of nuclear facilities." NUREG/CR-****, United States Nuclear Regulatory Commission, Washington, D.C.

Kumar, M., Whittaker, A. S., and Constantinou, M. C. (2015). "Seismic isolation of nuclear power plants using sliding bearings," MCEER-15-0006, University at Buffalo, The State University of New York, Buffalo, NY.

Kumar, M., Whittaker, A. S., Kennedy, R. P., Johnson, J. J., and Kammerer, A. M. (2016). "Seismic probabilistic risk assessment for safety-related nuclear facilities, " submitted to *Nuclear Engineering and Design*.

Livermore Software Technology Corporation (LSTC). (2013). "LS-DYNA keyword user's manual - Version R 7.0." Livermore, CA.

McVitty, W. J., and Constantinou, M. C. (2015). "Property modification factors for seismic isolators: design guidance for buildings." MCEER-15-0005, University at Buffalo, The State University of New York, Buffalo, NY.

Pacific Earthquake Engineering Research (PEER). (2011). "PEER ground motion database." http://peer.berkeley.edu/peer_ground_motion_database. (25th November, 2012), Berkeley, CA.

Reed, J. W. and Kennedy, R. P. (1994). "Methodology for developing seismic fragilities." TR-103959, Electric Power Research Institute, Palo Alto, CA.

Smith, P. D., Dong, R. G., Bernreuter, D. L., Bohn, M. P., Chuang, T. Y., Cummings, G. E., Johnson, J. J., Mensing, R. W., and Wells, J. E. (1981). "Seismic safety margins research program: phase 1 final report." NUREG/CR-2015, United States Nuclear Regulatory Commission, Washington, D.C.

Stevenson, J. D. (1978). "The economic effect of increased seismic load on nuclear power plant design and construction costs." *Nuclear Engineering and Design*, 48, 231-243.

Stevenson, J. D. (1981). "Evaluation of the cost effects on nuclear power plant construction resulting from the increase in seismic design level." NUREG/CR-1508, United States Nuclear Regulatory Commission, Washington, D.C.

Stevenson, J. D. (2003). "Historical development of the seismic requirements for construction of nuclear power plants in the U.S. and worldwide and their current impact on cost and safety." *Transactions of the 17th Conference on Structural Mechanics and Reactor Technology* (SMiRT-17), Prague, Czech Republic.

United States Geological Survey (USGS). (2008). "2008 Interactive deaggregations." http://geohazards.usgs.gov/deaggint/2008/, accessed 03/01/2016

United States Nuclear Regulatory Commission (USNRC). (2007). "A performance-based approach to define the site-specific ground motion." Regulatory Guide 1.208, Washington, D.C.

Yang, T. Y., Moehle, J. P., Stojadinovic, B., and Der Kiureghian, A. (2009)."*Journal of Structural Engineering*, 135(10), 1146-1154.